Ubiquitination-activated TAB–TAK1–IKK–NF-κB axis modulates gene expression for cell survival in the lysosomal damage response

(14 words, 125 characters)

Akinori Endo,[1, 4*] Chikage Takahashi,[1] Naoko Ishibashi,[1] Yasumasa Nishito,[2] Koji Yamano,[3] Keiji Tanaka,[1] Yukiko Yoshida[1*]

[1]Laboratory of Protein Metabolism, Tokyo Metropolitan Institute of Medical Science, Tokyo, 156-8506, Japan

[2]Technology Research Division, Tokyo Metropolitan Institute of Medical Science, Tokyo, 156-8506, Japan

[3]Intracellular quality control project, Tokyo Metropolitan Institute of Medical Science, Tokyo, 156-8506, Japan

[4]Lead contact

[*]Correspondence: endo-ak@igakuken.or.jp (A.E.), yoshida-yk@igakuken.or.jp (Y.Y.)

Abstract

The lysosomal damage response is important for the maintenance of cellular homeostasis. Although the mechanisms underlying the repair and autophagic elimination of damaged lysosomes have been elucidated, the early signal transduction pathways and genes induced in response to lysosomal damage remain elusive. We performed transcriptome and proteome analyses and found that the TAB–TAK1–IKK–NF-κB axis is activated by K63-linked ubiquitin chains that accumulate on damaged lysosomes. This activates the expression of various transcription factors and cytokines that promote anti-apoptosis and intercellular signaling. The findings highlight the crucial role of ubiquitin-regulated signal transduction and gene expression in cell survival and cell–cell communication in response to lysosomal damage. The results suggest that the ubiquitin system is not only involved in the removal of damaged lysosomes by lysophagy, but also functions in the activation of cellular signaling for cell survival.

(140 words)

Introduction

Lysosomes are the primary degradative organelles and play a pivotal role in maintaining cellular and tissue homeostasis[1,2]. Lysosomal dysfunction is associated with various diseases, underscoring the crucial role of lysosomal integrity and its quality control in human health[3-5]. Lysosomes are susceptible to damage by many sources, both internal and external to the cell, which results in the permeabilization and rupture of lysosomal membranes. Crystals, amyloids, pathogens, lipids, lysosomal toxic drugs, and reactive oxygen species (ROS) are among the stressors that can damage lysosomal membranes[6-10]. The release of enzymes and protons from the lumen of damaged lysosomes induces oxidative stress, inflammation, and cell death, which is deleterious to cells and tissues[10,11]. The accumulation of damaged lysosomes is thus an important factor involved in the development of aging-related diseases and other conditions such as crystalline nephropathy, neurodegenerative, and infectious diseases[3-5,12].

To overcome lysosomal damage and restore lysosomal functionality, cells have developed a set of response pathways that is collectively referred to as the lysosomal damage response[6,13]. It has been reported that signal mediators, such as AMP-activated protein kinase (AMPK) and mammalian target of rapamycin (mTOR), exert the signal transduction in the lysosomal damage response[14,15]. The quality control mechanisms for damaged lysosomes include repair, elimination, and regeneration. Lysosomal membrane damage triggers the recruitment of the endosomal sorting complex required for transport (ESCRT) to repair the damaged membrane[13,16]. Current studies have shown that endoplasmic reticulum (ER)-lysosome lipid transfer is crucial for lysosomal membrane

55 repair[17,18]. Furthermore, stress granules (SGs) have been demonstrated to play a pivotal role
56 in the repair process[19]. When the damage is extensive and repair is not feasible, the
57 damaged lysosome undergoes autophagic elimination in a process known as lysophagy[13,20].
58 In lysophagy, lysosomal membrane permeabilization leads to extensive ubiquitination of
59 exposed proteins. This triggers the recruitment of ubiquitin-binding autophagy receptors,
60 which activates autophagy to sequester and degrade damaged lysosomes[13,21]. Protein
61 ubiquitination is an important form of post-translational modification that is comparable to
62 protein phosphorylation. Protein ubiquitination in lysophagy occurs through the formation
63 of Lys-63-linked ubiquitin chains (K63 ubiquitin chains)[22]. Substrate ubiquitination in
64 damaged lysosomes is catalyzed by the E2 ubiquitin-conjugating enzyme UBE2QL1 and
65 several ubiquitin E3 ligases, including TRIM16, CUL1–SKP1–FBXO27, and CUL4A–
66 DDB1–WDFY1[23-26].

67 Transcription factor EB (TFEB), a master regulator of lysosome- and autophagy-related
68 gene expression, is activated during the repair and elimination of damaged lysosomes,
69 which results in the regeneration of lysosomes as part of the lysosomal damage response[27-
70 29]. Under unstimulated conditions, TFEB is phosphorylated by lysosome-associated
71 mTORC1 and binds to 14–3–3 proteins, resulting in the cytoplasmic retention of TFEB[30].
72 However, lysosomal permeabilization causes the dissociation of mTORC1 from lysosomes,
73 which leads to the dephosphorylation of TFEB and its translocation to the nucleus to
74 activate the expression of lysosome- and autophagy-related genes[3,14,30].

75 The elimination of damaged lysosomes through lysophagy requires a period of more
76 than half a day, during which the cell is vulnerable[31]. It is therefore assumed that there are

77 cellular mechanisms that cooperate with lysophagy to maintain cellular health in the
78 lysosomal damage response. In previous work, we demonstrated that K63 ubiquitin chains,
79 which accumulate on dysfunctional endosomes, induce cytokine production by modulating
80 gene expression in a TGF-beta-activated kinase 1 (TAK1) and TAK1-binding protein
81 (TAB) dependent manner[32,33]. K63 ubiquitin chains also accumulate in damaged lysosomes,
82 which serves as an initiating signal for lysophagy. This prompted us to investigate whether
83 gene expression is induced by ubiquitin-mediated activation of the TAB–TAK1 pathway in
84 the lysosomal damage response, as observed in the endosomal stress response. The
85 transcriptome of cells exposed to lysosomal damaging agents for 30 min has been
86 described[34]; however, genome-wide gene expression patterns associated with the lysosomal
87 damage response remain unclear. In this study, we performed transcriptome and proteome
88 analyses to comprehensively examine the regulation of gene expression in the lysosomal
89 damage response and to identify the underlying signal transduction pathways. We found
90 that accumulation of K63 ubiquitin chains in damaged lysosomes activates the TAB–
91 TAK1–IKK–NF-κB pathway, which in turn induces the expression of various transcription
92 factors and cytokines. We elucidated the critical role of the TAB–TAK1–IKK–NF-κB
93 pathway in cell survival and intercellular signal transduction. Collectively, the findings
94 suggest the existence of a universal response mechanism against the intracellular
95 accumulation of K63 ubiquitin chains.

Results

Lysosomal damage has a global impact on the transcriptome and proteome

To comprehensively investigate the changes in gene expression caused by lysosomal damage, we performed transcriptome analysis and compared mRNA expression between cells treated with L-Leucyl–L-Leucine methyl ester (LLOMe), a well-characterized inducer of lysosomal damage[35], and control cells. We used RPE-1 cells, which are commonly used in aging research. Transcriptome data revealed substantial alterations in gene expression in response to lysosomal damage. We identified >1,000 genes (946 upregulated and 164 downregulated genes from >13,000 transcripts with Log_2 fold change (FC) >|1| and P <0.05) that exhibited significant changes at 2 h after LLOMe treatment (Fig. 1A). Proteome analysis was performed to determine the correlation between proteomic changes and the observed alterations in the transcriptome. The analysis identified 86 upregulated and 60 downregulated proteins (of >10,000 proteins with Log_2 FC >|1| and P <0.05) (Fig. 1B). There was a modest correlation between the significant upregulation at the RNA level and that at the protein level, with a correlation coefficient (R) of 0.5899 from 302 data points (Fig. 1C and Fig. S1A). The representative targets interleukin-1 β (IL1β), IL6, interferon regulatory factor 1 (IRF1), and the proto-oncogenes c-Jun (JUN) and c-Fos (FOS) were upregulated at both the RNA and protein levels (Fig. 1C and S1A, B). This indicates that alterations in the transcriptome were, at least in part, responsible for those observed in the proteome. Genes showing significant upregulation in the transcriptome and proteome analyses were subjected to gene enrichment analysis using the Gene Ontology Molecular Function (GOMF) reference dataset (Fig. 1D, E). The results showed that these genes were

118 primarily enriched in transcription factors and cytokines (labeled in red and blue,
119 respectively, in Fig. 1D). Analysis using a Molecular Signatures Database (MSigDB)
120 hallmark gene set[36], a phenotypic reference dataset, indicated that genes upregulated at both
121 the RNA and protein levels were involved in biological regulatory processes including the
122 inflammatory response and apoptosis (Fig. 1E). It is noteworthy that the transcription factor
123 prediction using the DoRothEA regulon[37,38] identified the p65 (RELA) and p105 (NFKB1)
124 subunits of the NF-κB family as the primary transcription factors regulating gene
125 expression in the lysosomal damage response (Fig. 1F). This suggests that NF-κB
126 activation is involved in the regulation of gene expression in the lysosomal damage
127 response. The upregulation of IL1β, IL6, IRF1, JUN, and FOS at the protein level was
128 confirmed by immunoblotting (Fig. 1G).

129 Taken together, the results suggest that in the lysosomal damage response, the proteome
130 is remodeled according to alterations in the transcriptome; this remodeling is mediated
131 primarily through NF-κB and involves many transcription factors and cytokines, which
132 may potentially lead to the regulation of inflammation and apoptosis (Fig. 1H).

133

134 **Lysosomal damage activates TAK1 in a ubiquitin- and TAB-dependent manner**

135 Lysosomal membrane damage exposes glycoproteins, such as LAMP2. Cytosolic galectin
136 proteins, including Galectin-3 (Gal-3), are recruited to the lysosomal membrane by
137 recognizing beta-galactoside-containing glycans on exposed proteins. These exposed
138 lysosomal proteins are extensively ubiquitinated by ubiquitin ligases, resulting in the
139 accumulation of ubiquitinated proteins within damaged lysosomes[25,26,39]. An endosomal

140 stress response mechanism was recently described whereby K63 ubiquitin chains
141 accumulate on dysfunctional endosomes, activating TAK1 in a TAB-dependent manner[32].
142 TAB2 and TAB3 (a paralog of TAB2) function as ubiquitin decoders that specifically
143 recognize K63 ubiquitin chains via the C-terminal Npl4 zinc finger (NZF) domain[40,41]. The
144 finding that TAB binding to unanchored K63 ubiquitin chains is sufficient to activate TAK1
145 in vitro[42] suggests that the conjugation of K63 ubiquitin chains to bulky substrates on
146 endosomes is sufficient to facilitate TAB-dependent TAK1 activation. This prompted us to
147 investigate whether the accumulation of K63 ubiquitin chains in other regions of the
148 cytoplasm also results in TAK1 activation. TAK1 controls the function of the
149 p62/sequestosome, an autophagy receptor, and TAB2 undergoes TRIM38-mediated
150 lysosomal degradation in response to lysosomal damage[43,44]. However, whether TAK1 is
151 activated in a TAB-dependent manner and the role of the TAB–TAK1 signaling pathway in
152 the lysosomal damage response remain unanswered questions.

153 To determine whether the TAB–TAK1 signaling pathway is activated in response to
154 lysosomal damage, we initially examined the subcellular localization of TAB2 and TAK1.
155 The recruitment of Gal-3 and K63 ubiquitin chains to damaged lysosomes was confirmed
156 in RPE-1 cells (Fig. S2A-B). The co-localization of TAB2 and TAK1 with K63 ubiquitin
157 chains at damaged lysosomes was observed 5 min after LLOMe treatment (Fig. 2A). The
158 signals of LAMP1, a lysosomal marker protein, were enhanced, and LAMP1-positive
159 puncta were increased in size in RPE-1 cells treated with LLOMe. It is plausible that this
160 phenomenon reflects the morphological alterations in lysosomes under our experimental
161 conditions, possibly due to lysosomal membrane damage (Fig. 2A, S2A). Immunoblotting

162 analysis showed that the accumulation of K63 ubiquitin chains in the cell was accompanied
163 by an increase in active phosphorylated TAK1, which was first detected 5 min after
164 LLOMe treatment (Fig. 2B). TFEB isolated from cells treated with LLOMe exhibited a
165 downshift on the gel, which is a characteristic of TFEB activation[45]. This indicates that a
166 lysosomal damage response was activated under these experimental conditions (Fig. 2B).
167 TAK1 activation was abolished by the E1 ubiquitin-activating enzyme inhibitor TAK-243
168 and depletion of TAB2 and TAB3 (Fig. 2C, D). These results suggest that TAK1 is
169 activated in a ubiquitin- and TAB-dependent manner in the lysosomal damage response. To
170 further explore the potential involvement of K63 ubiquitination in TAK1 activation, we
171 performed an add-back experiment using siRNA-resistant TAB2 WT and mutants incapable
172 of binding to K63 ubiquitin chains, dNZF and E685A. The NZF domain of TAB2 is well-
173 characterized to specifically associate with K63 ubiquitin chains[40]. We investigated whether
174 the add-back of TAB2 mutants rescues the activation of TAK1 in TAB2-depleted cells (Fig.
175 2E). TAB2 WT, but not dNZF and E685A, restored TAK1 activation in response to
176 lysosomal damage, suggesting that the specific interaction of TAB proteins and K63
177 ubiquitin chains is a key mechanism to activate TAK1. Unexpectedly, the treatment of an
178 E1 inhibitor TAK-243 that abolished the lysosomal accumulation of K63 ubiquitin chains
179 did not inhibit the recruitment of TAB2 to damaged lysosomes, suggesting that the
180 recruitment of TAB proteins to damaged lysosomes is independent of the association with
181 K63 ubiquitin chains (Fig. S2B). Collectively, it is postulated that TAB proteins require the
182 interaction with K63 ubiquitin chains for TAK1 activation, but not for recruitment to
183 damaged lysosomes. We next examined whether other lysosomal damage inducers, Glycyl-

184 L-phenylalanine 2-naphthylamide (GPN) and DC661, also activate TAK1. It has been
185 shown that GPN and DC661 induce lysosomal membrane permeabilization through
186 hyperosmotic stress and lipid peroxidation in lysosomes, respectively[46,47]. In cells treated
187 with GPN and DC661, K63 ubiquitin chains were accumulated, possibly due to a defect in
188 the endo-lysosome machinery (Fig. S2C, D). However, the lysosomal accumulation of Gal-
189 3 was significantly lower than that observed in cells treated with LLOMe, suggesting that
190 GPN and DC661 did not induce severe lysosomal membrane permeabilization (Fig. S2C,
191 D). Under these conditions, the phosphorylation of TAK1 was not observed (Fig. S2E).
192 These findings indicate that the exposure of K63 ubiquitin chains within the cytosol
193 following severe lysosomal membrane permeabilization functions as an initial trigger for
194 TAB-mediated TAK1 activation in the lysosomal damage response.
195

196 **The TAB–TAK1 pathway plays a pivotal role in the induction of cytokines and**
197 **transcription factors in the lysosomal damage response**

198 To gain further insight into the involvement of the TAB–TAK1 pathway in the regulation of
199 gene expression associated with the lysosomal damage response, an additional
200 transcriptome analysis was performed on TAB- and TAK1-depleted cells treated with
201 LLOMe for 2 h. The genes upregulated in response to lysosomal damage were classified
202 into six distinct clusters within the dataset (Fig. 3A). Clusters 4 and 5 comprised genes that
203 are expressed in a TAB- and TAK1-dependent manner (Fig. 3A). Most of the genes
204 upregulated in a TAB- and TAK1-dependent manner showed overlapping expression
205 patterns (Fig. S3A, B); these genes were enriched for cytokines and growth factors, and

206 their functions were linked to inflammatory responses and apoptosis, as shown in the gene
207 enrichment analysis (Fig. S3C, D). Transcription factor prediction based on the DoRothEA
208 regulon indicated that genes in cluster 4, whose expression was inhibited by depletion of
209 TAB and TAK1, were targets of the NF-κB family, including RelA, NFKB1, and c-Rel
210 (REL) (Fig. 3B). The NF-κB family members were identified as the primary transcription
211 factors regulating gene expression in the lysosomal damage response (Fig. 1F). This
212 indicates that the TAB–TAK1 pathway serves as a primary axis for the activation of NF-κB
213 in the lysosomal damage response, thereby inducing target gene expression. Cytokines and
214 growth factors were enriched in cluster 4, and transcription factors were enriched in cluster
215 5, in which gene expression was partially suppressed (Fig. 3C, E). Regulators of the
216 inflammatory response and apoptotic functions were commonly enriched in clusters 4 and 5
217 (Fig. 3D). The results of immunoblotting showed that the protein expression of IL1β, IL6,
218 IRF1, homeobox protein Nkx-3.1 (NKX3.1), and JUN was consistent with the TAB- and
219 TAK1-mediated gene expression. Conversely, depletion of TAB and TAK1 did not affect
220 the expression of FOS at both the mRNA and protein levels (Fig. 3F and S3E).
221 Furthermore, the downshift of TFEB, which indicates the activation of TFEB, was not
222 affected by depletion of TAB and TAK1 (Fig. 3F). This suggests that TFEB activation is
223 independent of the TAB–TAK1 pathway in the lysosomal damage response.
224 In conclusion, transcriptome analysis in TAB- and TAK1-depleted cells indicates that the
225 TAB–TAK1 pathway induces the expression of cytokines and transcription factors,
226 potentially via NF-κB, in the lysosomal damage response, thereby regulating inflammatory
227 response and apoptosis.

228

229 **The K63 Ub–TAB–TAK1–IKK–NF-κB pathway is activated in the lysosomal damage**
230 **response**

231 To elucidate the downstream cascade of the TAB–TAK1 signaling pathway in the early
232 response to lysosomal damage, we performed proteome and phosphoproteome analyses
233 using the TAK1 inhibitor HS-276 (Fig. 4A, S4A). The phosphoproteome analysis showed
234 that the phosphorylation levels of stress-induced mitogen-activated protein kinases
235 (MAPKs), specifically p38α (MAPK14, pT180/pY182) and JNK3 (MAPK10, pY223), as
236 well as MK2 (MAPKAPK2, pT334), a downstream target of MAPKs, increased in
237 response to lysosomal damage, and this increase was dependent on TAK1 (Fig. S4B, C).
238 Phosphorylation of T180/Y182 in p38α and Y223 in JNK3 activates the kinase
239 function[48,49]. The TAK1-dependent phosphorylation of Y223 in JNK3 in the lysosomal
240 damage response was consistent with a previous report that lysosome rupture activates the
241 TAK1–JNK pathway in THP-1 cells[50]. Additionally, T334 of MK2 is a primary site of
242 phosphorylation by MAPKs[51]. These findings suggest that lysosomal damage induces
243 TAK1-dependent activation of MAPKs. Proteome analysis showed that the inhibitor of NF-
244 κB α (IκBα) undergoes TAK1-dependent degradation 30 min after LLOMe treatment (Fig.
245 4A, B). The inhibitor of NF-κB kinase (IKK) complex, which comprises IKKα, β, and γ,
246 functions downstream of TAK1 and phosphorylates IκBα, thereby inducing its
247 degradation[52]. Similarly, in response to ubiquitin-mediated endosomal stress, the NF-κB
248 pathway is activated in an IKK-dependent manner[32]. The degradation of IκBα is a hallmark
249 phenomenon upstream of NF-kB activation[53], which is primarily triggered by IKK-

mediated phosphorylation. This leads to the hypothesis that the IKK complex activated by the TAB–TAK1 pathway promotes the phosphorylation of IκBα, which leads to its degradation and NF-κB activation in the lysosomal damage response.

We therefore sought to characterize the kinase cascade that is activated in the lysosomal damage response. We confirmed the phosphorylation and subsequent degradation of IκBα (Fig. 4C). We also found that MAPKs and IKK were activated concomitant with a notable phosphorylation of IKK, JNK, and p38, and a relatively minimal phosphorylation of ERK (Fig. 4C). The increase in the phosphorylation levels of IKK, JNK, p38, and IκBα occurred in a ubiquitin-dependent manner, as the induction was abolished by TAK-243 (Fig. 4D). Depletion of TAB, TAK1, and IKK suppressed IκBα phosphorylation, and the phosphorylation of JNK and p38 was TAB- and TAK1-dependent (Fig. 4E, F). These findings indicate that the phosphorylation of IκBα is induced in a TAB–TAK1–IKK pathway-dependent manner. Additionally, it can be postulated that MAPKs, including JNK and p38, are activated by the TAB–TAK1 pathway.

TANK-binding kinase 1 (TBK1), a putative NF-κB regulator, has been reported to be activated in the lysosomal damage response[21]. We examined whether TBK1 coordinately functions with the TAB-TAK1 pathway to facilitate NF-κB activation. Consistent with the previous report, TBK1 was activated in response to LLOMe treatment (Fig. S4D). Depletion of TAB and TAK1 led to a slight reduction in the activation of TBK1 (Fig. S4E). The TBK1 inhibitor BX-795 did not affect TAK1 activation but abolished the phosphorylation of IKK and IκBα (Fig. S4F). With regard to the ubiquitination in the lysosomal damage response, the linear ubiquitin chain assembly complex (LUBAC)-

272 mediated M1 ubiquitination has been implicated in NF-κB activation[54]. To explore the
273 functional link between K63 and M1 ubiquitination, we examined the effects of LUBAC
274 depletion on the TAB-TAK1 pathway and the subsequent NF-κB activation. Depletion of
275 RNF31 (also known as HOIP), a component of LUBAC, exhibited no or minimal effects on
276 TAK1 activation, but abolished the phosphorylation of IKK and IκBα (Fig. S4G). These
277 findings suggest that TBK1 and LUBAC are indispensable for NF-κB activation in the
278 lysosomal damage response.

279 The IKK complex, which is activated by the TAB–TAK1 pathway in response to
280 lysosomal damage, has been shown to induce the phosphorylation and degradation of
281 IκBα, potentially leading to the activation of NF-κB (Fig. 4G). Furthermore, TBK1 and
282 LUBAC were required for NF-κB activation, but not for TAK1 activation, indicating that
283 TBK1 and LUBAC function downstream of or parallel to the TAB-TAK1 pathway.

284

285 **The K63 Ub–TAB–TAK1–NF-κB pathway regulates the expression of cytokines and**
286 **transcription factors essential for cell survival and intercellular signaling**

287 IL1β, IL6, IRF1, and NKX3.1 expression was associated with the lysosomal damage
288 response and dependent on the TAB–TAK1 pathway (Fig. 3E, F, and S3E). The expression
289 of these genes was suppressed by treatment with TAK-243 and HS-276 (Fig. 5A, B).
290 Depletion of IKKs suppressed target gene expression (Fig. 5C). These findings demonstrate
291 that the expression of these genes is induced by the ubiquitin-dependent activation of the
292 TAB–TAK1–IKK pathway in the lysosomal damage response.

293 Gene enrichment data based on the results of transcriptome and proteome analyses

294 indicated that TAB–TAK1 pathway-dependent gene expression plays a role in the
295 regulation of apoptosis and the inflammatory response (Fig. 3D and S3D). We thus
296 examined the impact of the K63 Ub–TAB–TAK1–IKK–NF-κB pathway on these cellular
297 functions. Lysosomal damage for 8 h did not induce apoptosis; however, inhibition of
298 ubiquitination by TAK-243 dramatically induced apoptosis in HeLa and RPE-1 cells (Fig.
299 5D, E, S5A). This indicates that ubiquitination is essential for cell survival in the lysosomal
300 damage response. Similarly, inhibition of TAK1 by HS-276 and depletion of TAB, TAK1,
301 and IKKs following lysosomal damage for 24 h promoted apoptosis in HeLa cells (Fig. 5D-
302 G). TAK1 inhibition induced apoptosis in RPE-1 cells to a lesser extent compared to HeLa
303 cells (Fig. 5D, E, S5A). In addition, the inhibition of JNK by JNK-IN-8 promoted apoptosis
304 following lysosomal damage for 12 h, which is a later time point than TAK-243 and HS-
305 276 (Fig. S5B). These findings demonstrate that the K63 Ub–TAB–TAK1 pathway
306 coordinately exerts anti-apoptotic effects through the downstream effectors such as IKK
307 and JNK in response to lysosomal damage, thereby promoting cell survival.

308 We further investigated the potential autocrine/paracrine-like effects of cytokines such
309 as IL1β and IL6, which are expected to be secreted outside the cells due to their
310 upregulation in the lysosomal damage response. IL6 activates the JAK–STAT pathway,
311 which is accompanied by the phosphorylation of STAT3[55]. Stimulation of untreated cells
312 with conditioned media (CM) from lysosome-damaged cells resulted in the
313 phosphorylation of STAT3, which indicates kinase activation (Fig. 5H). These results
314 suggest that the lysosomal damage response activates intercellular signaling involving the
315 JAK–STAT pathway. Furthermore, the capacity to activate this intercellular signaling was

316 decreased by depletion of TAB, TAK1, and IKKs (Fig. 5I, J).

317 Collectively, these findings suggest that the K63 Ub–TAB–TAK1 pathway plays a

318 pivotal role in cell survival and intercellular signaling in response to lysosomal damage.

Discussion

In this study, comprehensive analyses of the transcriptome and proteome demonstrated that lysosomal damage causes substantial alterations in gene expression, leading to proteome remodeling. Furthermore, we identified the signal transduction pathway mediating this response (Fig. 6). The accumulation of K63 ubiquitin chains in damaged lysosomes activates the TAB–TAK1–IKK–NF-κB pathway, which induces the expression of various transcription factors and cytokines. The present findings suggest that the ubiquitin-dependent signaling pathway plays a regulatory role in cell survival and intercellular signaling in the lysosomal damage response.

Prior to this study, our understanding of the lysosomal damage response was largely limited to the processes of repair and elimination of damaged lysosomes, as well as the activation and function of TFEB in lysosomal regeneration. Recent findings highlighting the role of stress granule formation in the lysosomal damage response suggest that additional pathways are involved in this process beyond what was previously anticipated[34]. Nevertheless, the complete picture remains to be elucidated. This study provides new information on the regulation of gene expression and signal transduction in the lysosomal damage response that offers a novel perspective for future research.

Aberrations in the lysosomal damage response are relevant to the pathogenesis of various age-related diseases, including neurodegenerative diseases[3,56]. In the context of pathology, inflammation, which is associated with numerous diseases, is linked to lysosomes. The inflammatory response is not only regulated by lysosomal function, but also triggered by lysosomal damage, and observed in lysosomal storage diseases[57,58]. The NLRP3

341 inflammasome induces an inflammatory response upon lysosomal damage by increasing
342 cytokine processing at the protein level[58,59]. The ubiquitin-regulated gene expression of pro-
343 inflammatory cytokines such as IL1β and IL6 may be involved in the induction of
344 inflammation in the lysosomal damage response, in addition to the regulation at the stage of
345 precursor processing. The present data on the regulation of gene expression by ubiquitin-
346 mediated signal transduction may help elucidate the molecular mechanisms underlying
347 diseases associated with lysosome dysfunction.

348 In this study, we demonstrated a pivotal role of the ubiquitin system in regulating gene
349 expression in the lysosomal damage response, which extends its function beyond that in
350 lysophagy initiation. We found that activation of the TAB–TAK1–IKK–NF-κB pathway,
351 potentially by the accumulation of K63 ubiquitin chains in damaged lysosomes, and the
352 subsequent induction of gene expression are crucial for cell survival and cell–cell
353 communication in cultured cells. Further analysis is required to determine the impact of this
354 action on disease pathogenesis and the maintenance of cellular homeostasis in organisms.

355 While we mainly focused on the TAB–TAK1–IKK–NF-κB pathway in this study, it
356 should be noted that TAK1 also activates AMPK, subsequently promoting lysophagy[15].
357 AMPK activation by TAK1 may also contribute to NF-κB activation or distinct gene
358 regulation. We found that TBK1 is required for NF-κB activation. In considering signal
359 mediators such as AMPK and TBK1, it is postulated that cell homeostasis is cooperatively
360 controlled by a set of regulators in the lysosomal damage response. A recent study
361 demonstrated that linear ubiquitin chains formed by LUBAC and deubiquitinated by
362 OTULIN activate NF-κB in the lysosomal damage response[54]. We have confirmed that

363 LUBAC is essential for NF-κB activation under our experimental conditions. It is well-
364 documented that LUBAC-catalyzed M1 ubiquitin chains recruit IKK subunits and
365 transduce the signaling to downstream mediators in the canonical pathway. Therefore, we
366 hypothesized that K63 ubiquitin chains in damage lysosomes initially activate the TAB–
367 TAK1 pathway and trigger LUBAC-mediated M1 ubiquitination. We further postulate that
368 M1 ubiquitination subsequently recruits the IKK complex to damaged lysosomes.
369 Consequently, activated TAK1 phosphorylates IKK subunits, leading to NF-kB activation
370 (Fig. 6). Apart from the lysosomal damage response, activated STING at the Golgi also
371 leads to NF-κB activation through LUBAC-mediated formation of linear ubiquitin chains[60].
372 In addition, the IKK complex is recruited to damaged mitochondria, potentially through its
373 association with accumulated ubiquitin chains, and activates NF-κB[61]. Although the
374 involvement of the TAB–TAK1 pathway was not examined in these studies, a common
375 mechanism underlying NF-κB activation induced by the accumulation of ubiquitin on
376 damaged or stressed organelles may serve as a unifying determinant. Taken together with
377 our previous findings that the accumulation of K63 ubiquitin chains in dysfunctional
378 endosomes induces cytokine expression via the TAB–TAK1 pathway[32], the present results
379 suggest the existence of a universal response to the intracellular accumulation of K63
380 ubiquitin chains resulting from fluctuations in the cellular environment, including organelle
381 stress. This universal response would entail the activation of NF-κB and the modulation of
382 downstream target gene expression for the regulation of cellular functions that maintain
383 homeostasis.

Materials and methods

Cell culture

RPE-1 cells were cultured at 37°C under 5% CO_2 in Dulbecco's Modified Eagle Medium (DMEM) / Ham's F-12 (WAKO, 048-29785) supplemented with 10% fetal bovine serum (FBS, Nichirei, 175013), 1 mM sodium pyruvate (Thermo Fisher Scientific, 11360070), 1× nonessential amino acids (Thermo Fisher Scientific, 11140050), and 1× Penicillin–Streptomycin–Glutamine (Thermo Fisher Scientific, 10378016). HeLa cells were cultured at 37°C under 5% CO_2 in DMEM (Thermo Fisher Scientific, D5796) supplemented with 10% FBS, 1 mM sodium pyruvate, 1× nonessential amino acids, and 1× Penicillin–Streptomycin–Glutamine. For experiments using conditioned medium, RPE-1 cells were stimulated with culture medium from RPE-1 cells that had been treated with or without 1 mM L-Leucyl–L-Leucine methyl ester (LLOMe, Cayman, 16008). At 30 min after treatment, the LLOMe was washed out and cells were further incubated in DMEM supplemented with 0.5% FBS, 1 mM sodium pyruvate, 1× nonessential amino acids, and 1× Penicillin–Streptomycin–Glutamine for 8 h. HeLa cells stably expressing siRNA-resistant FLAG-TAB2 WT, dNZF, and E685A were generated previously[32].

Reagents and inhibitors

To induce lysosomal damage, cells were treated with 1 mM LLOMe, 200 μM Glycyl-L-phenylalanine 2-naphthylamide (GPN, Cayman, 14634), and DC661 (Cayman, 34899) for the indicated times. In the event of a longer incubation period, the LLOMe was washed out

405 2 h after treatment. The following inhibitors were used in this study: TAK-243 (10 μM,
406 Active Biochem, A-1384), HS-276 (10 μM, Sigma-Aldrich, SML-3629), BX-795 (2 μM,
407 Abcam, ab142016), and JNK-IN-8 (10 μM, Cayman, 18096).

408

409 **Transcriptome analysis**

410 Total RNA from RPE-1 cells was prepared using the Qiashredder kit (Qiagen, 79654), the
411 RNeasy kit (Qiagen, 74104), and DNase (Qiagen, 79254). The quality of RNA samples was
412 assessed using an Agilent 2100 bioanalyzer (Agilent Technologies); an RNA integrity
413 number >9 was recorded for all samples. A total of 500 ng of each sample was processed
414 with the Illumina Stranded mRNA Prep kit, and indexes were added with the IDT for
415 Illumina RNA UD Indexes Set A (Illumina). The average library size was estimated using
416 the Agilent 2100 Bioanalyzer, and libraries were quantified using a Qubit Fluorometer
417 (Thermo Fisher Scientific). Samples were pooled into a single library and sequenced using
418 the NextSeq 1000/2000 P2 Reagents (300 cycles, paired-end 150bp) on the Illumina
419 NextSeq 1000 system. Sequence data were analyzed using the onboard DRAGEN RNA
420 Pipeline Application (v.3.10.12).

421

422 **Proteome analysis**

423 RPE-1 cells were lysed in 5% SDS lysis buffer [5% SDS and 50 mM triethylammonium
424 bicarbonate (TEAB, Thermo Fisher Scientific, 90114), followed by sonication with an

ultrasonication probe. Cell lysates were reduced and alkylated with 4.5 mM dithiothreitol (DTT, Thermo Fisher Scientific, A39255) for 30 min at 55°C and 10 mM iodoacetamide (IAA, Thermo Fisher Scientific, A39271) for 15 min at room temperature (RT). Subsequently, 30 μg of cell lysates were loaded onto S-Trap micro columns (ProtiFi, C02-micro); trypsin and lysyl-endopeptidase (Lys-C) solution (1:10 w/w, Thermo Fisher Scientific, A41009) was added and incubated for 16 h at 37°C. The eluted peptides were dried in a vacuum concentrator and resuspended in 0.1% trifluoroacetic acid (TFA). Aliquots containing 500 ng of peptides from each sample were loaded onto a Vanquish Neo UHPLC system-connected Orbitrap Exploris 480 mass spectrometer (Thermo Fisher Scientific). The peptides were separated on an analytical column (C18, 1.7 μm particle size × 75 μm diameter × 600 mm, IonOpticks, AUR3-60075C18) heated at 55°C in a column oven (Sonation, PRSO-C2) with a constant flow rate of 250 nL/min. The peptides were eluted with a 0–40% acetonitrile gradient over 120 min. Peptide ionization was performed using the Nanospray Flex Ion Source (Thermo Fisher Scientific). The Orbitrap Exploris 480 mass spectrometer was operated in data-independent acquisition (DIA) mode using a full scan (m/z range of 380–985, nominal resolution of 60,000, and target value of 3×10^6 ions) followed by DIA-MS scans (fixed collision energy of 30%, isolation width of 10 m/z with an overlapping of 1 m/z, nominal resolution of 15,000, and target value of 2×10^6 ions).

DIA-MS data processing and visualization

The MS raw files were searched against the human UniProt reference proteome (Uniprot ID: UP000005640, reviewed, canonical, 20,563 entries) in library-free mode using DIA-NN software (version 1.9.1)[62]. The parameters that differed from the default settings were as follows: variable modifications, oxidation of methionine and acetylation of the peptide N-terminus; precursor m/z range, 380–985. Following processing with DIA-NN, the exported data were subjected to imputation using Perseus software[63]. The default setting was used, assuming that missing values represent low protein abundance. In this case, missing values were replaced by random numbers drawn from a normal distribution across the entire matrix. Gene enrichment tests and clustering were performed using the RNAseqChef software[64], and heatmaps were generated using the Morpheus platform (https://software.broadinstitute.org/morpheus/). The volcano plots, scatter plots, and bar graphs were visualized using GraphPad Prism software (version 8.1.0, GraphPad).

Cell lysis and immunoblotting

Cells were lysed with 2% SDS lysis buffer (2% SDS, 20 mM HEPES pH 7.5, 1 mM EDTA) containing a complete protease inhibitor cocktail (EDTA-free, Roche, 05056489001) and a phosphatase inhibitor cocktail (Roche, 4906845001). Cell lysates were boiled in 1× LDS NuPAGE sample buffer (Thermo Fisher Scientific, NP0008) for 10 min at 70°C, and then electrophoresed on 4–12% NuPAGE Bis-Tris gels (Thermo Fisher Scientific). Proteins were transferred to polyvinylidene difluoride membranes (Millipore, IPVH00010 or Pall, EH-2222). The membranes were incubated with 5% nonfat milk for 1 h at RT, followed by incubation for 2 h at RT with primary antibodies. The primary

468 antibodies used for immunoblotting were anti-IL1β mouse monoclonal (Cell Signaling
469 Technology, 12242), anti-IL6 rabbit monoclonal (Cell Signaling Technology, 12153), anti-
470 IRF1 rabbit monoclonal (Cell Signaling Technology, 8478), anti-NKX3.1 rabbit
471 monoclonal (Cell Signaling Technology, 92998), anti-c-Fos rabbit monoclonal (Cell
472 Signaling Technology, 2250), anti-c-Jun rabbit monoclonal (Cell Signaling Technology,
473 9165), HRP-conjugated anti-α-tubulin rabbit polyclonal (MBL, PM054-7), anti-K63
474 ubiquitin rabbit monoclonal (Millipore, 05-1308), anti-ubiquitin mouse monoclonal (Santa
475 Cruz Biotechnology, sc-8017), anti-phospho-TAK1 (T184/T187) rabbit monoclonal (Cell
476 Signaling Technology, 4508), anti-TAK1 rabbit polyclonal (Cell Signaling Technology,
477 4505), anti-TAB2 rabbit polyclonal (Abcam, ab222214), anti-TAB3 rabbit polyclonal
478 (Abcam, ab85655), HRP-conjugated anti-FLAG mouse monoclonal (Sigma-Aldrich,
479 A8592), anti-TFEB rabbit monoclonal (Cell Signaling Technology, 37785), anti-phospho-
480 IKKα/β (S176/S180) rabbit monoclonal (Cell Signaling Technology, 2697), anti-IKKα
481 rabbit polyclonal (Cell Signaling Technology, 2682), anti-IKKβ rabbit monoclonal (Cell
482 Signaling Technology, 8943), anti-phospho-IκBα (S32) rabbit monoclonal (Cell Signaling
483 Technology, 2859), anti-IκBα rabbit monoclonal (Cell Signaling Technology, 4812), anti-
484 phospho-JNK (T183/Y185) rabbit monoclonal (Cell Signaling Technology, 4668), anti-
485 JNK rabbit polyclonal (Cell Signaling Technology, 9252), anti-phospho-p38 (T180/Y182)
486 rabbit polyclonal (Cell Signaling Technology, 9211), anti-p38 rabbit monoclonal (Cell
487 Signaling Technology, 8690), anti-phospho-ERK (T202/Y204) rabbit monoclonal (Cell
488 Signaling Technology, 4370), anti-ERK rabbit monoclonal (Cell Signaling Technology,
489 4695), anti-cleaved caspase-3 rabbit polyclonal (Cell Signaling Technology, 9661), anti-

phospho-STAT3 (Y705) rabbit monoclonal (Cell Signaling Technology, 9145), anti-STAT3 rabbit monoclonal (Cell Signaling Technology, 4904), anti-phospho-TBK1 (S172) rabbit monoclonal (Cell Signaling Technology, 5483), anti-TBK1 rabbit monoclonal (Abcam, ab40676), and anti-RNF31 rabbit monoclonal (Cell Signaling Technology, 99633) antibodies. The membranes were then incubated with secondary antibodies for 50 min at RT. The secondary antibodies used were HRP-conjugated goat anti-rabbit Ig (Promega, W4011) and anti-mouse Ig (Promega, W4021). The antibodies were diluted with Can Get Signal Solutions (TOYOBO, NKB-101). Chemiluminescence images were developed using the ECL Prime Western Blotting Detection Reagent (Cytiva, RPN2236) and acquired with a Fusion FX7 (Vilber Bio Imaging).

Phosphoproteome analysis

RPE-1 cells were treated with or without 1 mM LLOMe and 10 μM HS-276 for the indicated times, after which they were lysed, reduced, and alkylated as described above (proteome analysis). Aliquots containing 200 μg of lysate were loaded onto S-Trap mini columns (ProtiFi, C02-mini), followed by the addition of the trypsin solution (1:10 w/w, Cell Signaling Technology, 56296) and incubation for 16 h at 37°C. The eluted peptides were dried in a vacuum concentrator. Phosphopeptides were enriched using the High-Select Fe-NTA Phosphopeptide Enrichment Kit (Thermo Fisher Scientific, A32992) and dried in a vacuum concentrator. The resultant peptides were cleaned using C18 spin tips (Thermo Fisher Scientific, 84850), dried in a vacuum concentrator, resuspended in 0.1% TFA, and

511 loaded onto a Vanquish Neo UHPLC system-connected Orbitrap Exploris 480 mass
512 spectrometer. The peptides were separated on an analytical column (C18, 1.7 μm particle
513 size × 75 μm diameter × 250 mm, IonOpticks, AUR3-25075C18) heated at 55°C in a
514 column oven with a constant flow rate of 250 nL/min. The peptides were eluted with a 0–
515 40% acetonitrile gradient over 120 min. Peptide ionization was performed using the
516 Nanospray Flex Ion Source. The Orbitrap Exploris 480 mass spectrometer was operated in
517 data-dependent acquisition (DDA) mode utilizing a full scan (m/z range, 375–1500;
518 nominal resolution, 60,000; target value, 3×10^6 ions) followed by MS/MS scans (fixed
519 collision energy, 30%; isolation width, 1.6 m/z; nominal resolution, 15,000, and target
520 value, 1×10^5 ions). Precursor ions selected for fragmentation (charge state 2–6) were
521 placed on a dynamic exclusion list for 20 s. A "1-s cycle" DDA method was used, whereby
522 the most intense ions were selected every second for MS/MS fragmentation by higher-
523 energy collisional dissociation.

524

525 **DDA-MS data processing and visualization**

526 The MS raw files were searched against the human UniProt reference proteome (Uniprot
527 ID: UP000005640, reviewed, canonical, 20,563 entries) using the Sequest HT search
528 program in Proteome Discoverer 3.1 (Thermo Fisher Scientific). Intensity-based non-label
529 quantification was performed using the Precursor Ions Quantifier node in Proteome
530 Discoverer 3.1. Volcano plots, scatter plots, and bar graphs were visualized using GraphPad
531 Prism (version 8.1.0, GraphPad).

532

533 **Immunofluorescence and confocal microscopy analysis**

534 Cells were plated in 35-mm glass-bottomed dishes coated with poly-L-lysine (MatTek,
535 P35-GC-0-10-C). They were fixed with 4% paraformaldehyde in PBS for 10 min at RT and
536 permeabilized with 0.2% Triton X-100 in PBS for 5 min at RT. Alternatively, the cells were
537 incubated with ice-cold methanol for 10 min on ice. Following incubation with 5% FBS
538 and 0.1% Tween in PBS for 30 min at RT, cells were incubated with primary antibodies for
539 2 h at RT and then stained with secondary antibodies and DAPI (Thermo Fisher Scientific,
540 D1306) for 1 h at RT. The following primary antibodies were used: anti-TAB2 mouse
541 monoclonal (Santa Cruz Biotechnology, sc-398188), anti-LAMP1 rabbit monoclonal (Cell
542 Signaling Technology, 9091), anti-K63 ubiquitin rabbit monoclonal (Millipore, 05-1308),
543 anti-TAK1 mouse monoclonal (Santa Cruz Biotechnology, sc-7967), and anti-Galectin-3 rat
544 monoclonal (Santa Cruz Biotechnology, sc-23938). The following secondary antibodies
545 were purchased from Thermo Fisher Scientific: Alexa Fluor 488-conjugated anti-mouse (A-
546 11029) and anti-rat (A-11006); and Alexa Fluor 594-conjugated anti-rabbit (A-11012).
547 After staining, the cells were coverslipped (Matsunami, C015001) with SlowFade Gold
548 (Thermo Fisher Scientific, S36936). Images were captured using ZEN 3.8 imaging software
549 and LSM980 laser-scanning confocal microscopes equipped with a Plan-Apochromat
550 63×/1.4NA oil lens (Carl Zeiss).

551

552 **Small interfering RNA (siRNA) transfection**

553 Cells were transfected with siRNAs using Lipofectamine RNAiMax (Thermo Fisher
554 Scientific) at a final siRNA concentration of 30 nM. Cells were harvested and analyzed 72
555 h after transfection with siRNA. The siRNAs utilized pools of four different sequences
556 (Horizon Discovery). The following siRNAs were used: TAB2 siRNAs: L-004771; TAB3
557 siRNAs: L-015572; TAK1 siRNAs: L-003790; IKKα siRNAs: L-003473; IKKβ siRNAs:
558 L-003503; IKKγ siRNAs: L-003763; and RNF31 siRNAs: L-021419.
559

560 **RT-qPCR analysis**

561 Total RNA was extracted using NucleoSpin RNA Plus (MACHEREY-NAGEL,
562 740984.250). cDNA was generated using the ReverTra Ace qPCR RT Master Mix with
563 gDNA Remover kit (TOYOBO, FSQ-301). Quantification of mRNA was performed using
564 a Light Cycler 480 (Roche) with THUNDERBIRD SYBR qPCR Mix (TOYOBO, QPS-
565 201) as the detection reagent. The primer sets used for qRT-PCR were as follows: IL1β
566 forward: TACGATCACTGAACTGCACGC, IL1β reverse:
567 CTTGTTGCTCCATATCCTGTCCC; IL6 forward: TCATCACTGGTCTTTTGGAGTTTG,
568 IL6 reverse: CAGCTCTGGCTTGTTCCTCAC; IRF1 forward:
569 GCCATTCACACAGGCCGATAC, IRF1 reverse: TGCTCTGGTCTTTCACCTCCTC;
570 NKX3.1 forward: CTGGGAGACTTGGAGAAGCAC, NKX3.1 reverse:
571 GGATAGCTGTTATACACGGAGACC; and GAPDH forward:
572 AGAAGGTGGTGAAGCAGGCG, GAPDH reverse:
573 CAAAGTGGTCGTTGAGGGCAATG.

Cell death assay

Cell death upon lysosomal damage was assessed by propidium iodide (PI) staining. Both cells attached to the culture dish and suspended in media were collected and stained with 50 μg/mL of PI (Thermo Fisher Scientific, P3566) for 15 min at RT. After washing excess PI, cells were resuspended in fresh PBS. Stained cells were loaded and counted on LSR-Fortessa (BD Biosciences).

Statistical analysis

Statistical analysis was performed using GraphPad Prism (version 8.1.0). All statistical information is provided in the figure legends. First, the sample distribution was assessed using the Shapiro–Wilk test. In the absence of formal testing, datasets with small sample sizes were assumed to have a normal distribution. The unpaired two-tailed Student's t-test was used to determine statistical significance when comparing unpaired two independent groups with normal distribution and no significant difference in standard deviation (SD). For multiple comparisons involving more than two unpaired groups with normal distribution, an ordinary one-way ANOVA with Dunnett's multiple comparison test was used. In all instances, statistical significance was evaluated with a 95% confidence interval, and a P value <0.05 was considered statistically significant.

Data availability

The RNA sequencing data have been deposited with links to BioProject accession number PRJDB19809 in the BioProject database of DNA Data Bank of Japan (DDBJ). The mass spectrometry proteomics data have been deposited to the ProteomeXchange Consortium via the PRIDE partner repository[65] with dataset identifiers PXD058072 (related to Fig. 1B–E and S1A, B), PXD058075 (related to Fig. 4A, B), and PXD058080 (related to Fig. S4A–C).

Acknowledgements

This research was supported by JSPS KAKENHI (grant no. JP18K14623 and JP20K06568 to A.E., JP23H04923 and JP23K23841 to K.Y., and JP23H04921 to K.T.) and AMED (grant no. JP21gm6410012 to A.E.).

Author contributions

The study was conceived by Akinori Endo, Keiji Tanaka, and Yukiko Yoshida. Transcriptome analyses were performed by Yasumasa Nishito. Proteome analyses were performed by Akinori Endo. Microscopy analyses were performed by Akinori Endo. Biochemical experiments were performed by Akinori Endo, Chikage Takahashi, Naoko Ishibashi, and Koji Yamano. Writing and editing were performed by Akinori Endo and Yukiko Yoshida.

Declaration of interest

The authors declare no competing financial interests.

REFERENCES

1. Ballabio, A., and Bonifacino, J.S. (2020). Lysosomes as dynamic regulators of cell and organismal homeostasis. Nat Rev Mol Cell Biol *21*, 101-118. 10.1038/s41580-019-0185-4.
2. Yang, C., and Wang, X. (2021). Lysosome biogenesis: Regulation and functions. J Cell Biol *220*. 10.1083/jcb.202102001.
3. Tan, J.X., and Finkel, T. (2023). Lysosomes in senescence and aging. EMBO Rep *24*, e57265. 10.15252/embr.202357265.
4. Settembre, C., and Perera, R.M. (2024). Lysosomes as coordinators of cellular catabolism, metabolic signalling and organ physiology. Nat Rev Mol Cell Biol *25*, 223-245. 10.1038/s41580-023-00676-x.
5. Bonam, S.R., Wang, F., and Muller, S. (2019). Lysosomes as a therapeutic target. Nat Rev Drug Discov *18*, 923-948. 10.1038/s41573-019-0036-1.
6. Papadopoulos, C., and Meyer, H. (2017). Detection and Clearance of Damaged Lysosomes by the Endo-Lysosomal Damage Response and Lysophagy. Curr Biol *27*, R1330-R1341. 10.1016/j.cub.2017.11.012.
7. Cantuti-Castelvetri, L., Fitzner, D., Bosch-Queralt, M., Weil, M.T., Su, M., Sen, P., Ruhwedel, T., Mitkovski, M., Trendelenburg, G., Lütjohann, D., et al. (2018). Defective cholesterol clearance limits remyelination in the aged central nervous system. Science *359*, 684-688. 10.1126/science.aan4183.
8. Mossman, B.T., and Churg, A. (1998). Mechanisms in the pathogenesis of asbestosis and silicosis. Am J Respir Crit Care Med *157*, 1666-1680. 10.1164/ajrccm.157.5.9707141.
9. Gómez-Sintes, R., Ledesma, M.D., and Boya, P. (2016). Lysosomal cell death mechanisms in aging. Ageing Res Rev *32*, 150-168. 10.1016/j.arr.2016.02.009.
10. Wang, F., Gomez-Sintes, R., and Boya, P. (2018). Lysosomal membrane permeabilization and cell death. Traffic *19*, 918-931. 10.1111/tra.12613.
11. Hornung, V., Bauernfeind, F., Halle, A., Samstad, E.O., Kono, H., Rock, K.L., Fitzgerald, K.A., and Latz, E. (2008). Silica crystals and aluminum salts activate the NALP3 inflammasome through phagosomal destabilization. Nat Immunol *9*, 847-856. 10.1038/ni.1631.
12. Nakamura, S., Shigeyama, S., Minami, S., Shima, T., Akayama, S., Matsuda, T.,

Esposito, A., Napolitano, G., Kuma, A., Namba-Hamano, T., et al. (2020). LC3 lipidation is essential for TFEB activation during the lysosomal damage response to kidney injury. Nat Cell Biol *22*, 1252-1263. 10.1038/s41556-020-00583-9.

13. Meyer, H., and Kravic, B. (2024). The Endo-Lysosomal Damage Response. Annu Rev Biochem *93*, 367-387. 10.1146/annurev-biochem-030222-102505.

14. Jia, J., Abudu, Y.P., Claude-Taupin, A., Gu, Y., Kumar, S., Choi, S.W., Peters, R., Mudd, M.H., Allers, L., Salemi, M., et al. (2018). Galectins Control mTOR in Response to Endomembrane Damage. Mol Cell *70*, 120-135 e128. 10.1016/j.molcel.2018.03.009.

15. Jia, J., Bissa, B., Brecht, L., Allers, L., Choi, S.W., Gu, Y., Zbinden, M., Burge, M.R., Timmins, G., Hallows, K., et al. (2020). AMPK, a Regulator of Metabolism and Autophagy, Is Activated by Lysosomal Damage via a Novel Galectin-Directed Ubiquitin Signal Transduction System. Mol Cell *77*, 951-969 e959. 10.1016/j.molcel.2019.12.028.

16. Radulovic, M., Schink, K.O., Wenzel, E.M., Nahse, V., Bongiovanni, A., Lafont, F., and Stenmark, H. (2018). ESCRT-mediated lysosome repair precedes lysophagy and promotes cell survival. EMBO J *37*. 10.15252/embj.201899753.

17. Wang, X., Xu, P., Bentley-DeSousa, A., Hancock-Cerutti, W., Cai, S., Johnson, B.T., Tonelli, F., Shao, L., Talaia, G., Alessi, D.R., et al. (2025). The bridge-like lipid transport protein VPS13C/PARK23 mediates ER-lysosome contacts following lysosome damage. Nat Cell Biol *27*, 776-789. 10.1038/s41556-025-01653-6.

18. Radulovic, M., Wenzel, E.M., Gilani, S., Holland, L.K., Lystad, A.H., Phuyal, S., Olkkonen, V.M., Brech, A., Jaattela, M., Maeda, K., et al. (2022). Cholesterol transfer via endoplasmic reticulum contacts mediates lysosome damage repair. EMBO J *41*, e112677. 10.15252/embj.2022112677.

19. Bussi, C., Mangiarotti, A., Vanhille-Campos, C., Aylan, B., Pellegrino, E., Athanasiadi, N., Fearns, A., Rodgers, A., Franzmann, T.M., Saric, A., et al. (2023). Stress granules plug and stabilize damaged endolysosomal membranes. Nature *623*, 1062-1069. 10.1038/s41586-023-06726-w.

20. Papadopoulos, C., Kravic, B., and Meyer, H. (2020). Repair or Lysophagy: Dealing with Damaged Lysosomes. J Mol Biol *432*, 231-239. 10.1016/j.jmb.2019.08.010.

21. Eapen, V.V., Swarup, S., Hoyer, M.J., Paulo, J.A., and Harper, J.W. (2021). Quantitative proteomics reveals the selectivity of ubiquitin-binding autophagy receptors in the turnover of damaged lysosomes by lysophagy. Elife *10*. 10.7554/eLife.72328.

22. Gahlot, P., Kravic, B., Rota, G., van den Boom, J., Levantovsky, S., Schulze, N.,

Maspero, E., Polo, S., Behrends, C., and Meyer, H. (2024). Lysosomal damage sensing and lysophagy initiation by SPG20-ITCH. Molecular Cell. 10.1016/j.molcel.2024.02.029.

23. Chauhan, S., Kumar, S., Jain, A., Ponpuak, M., Mudd, M.H., Kimura, T., Choi, S.W., Peters, R., Mandell, M., Bruun, J.A., et al. (2016). TRIMs and Galectins Globally Cooperate and TRIM16 and Galectin-3 Co-direct Autophagy in Endomembrane Damage Homeostasis. Dev Cell *39*, 13-27. 10.1016/j.devcel.2016.08.003.

24. Koerver, L., Papadopoulos, C., Liu, B., Kravic, B., Rota, G., Brecht, L., Veenendaal, T., Polajnar, M., Bluemke, A., Ehrmann, M., et al. (2019). The ubiquitin-conjugating enzyme UBE2QL1 coordinates lysophagy in response to endolysosomal damage. EMBO Rep *20*, e48014. 10.15252/embr.201948014.

25. Yoshida, Y., Yasuda, S., Fujita, T., Hamasaki, M., Murakami, A., Kawawaki, J., Iwai, K., Saeki, Y., Yoshimori, T., Matsuda, N., and Tanaka, K. (2017). Ubiquitination of exposed glycoproteins by SCF(FBXO27) directs damaged lysosomes for autophagy. Proc Natl Acad Sci U S A *114*, 8574-8579. 10.1073/pnas.1702615114.

26. Teranishi, H., Tabata, K., Saeki, M., Umemoto, T., Hatta, T., Otomo, T., Yamamoto, K., Natsume, T., Yoshimori, T., and Hamasaki, M. (2022). Identification of CUL4A-DDB1-WDFY1 as an E3 ubiquitin ligase complex involved in initiation of lysophagy. Cell Rep *40*, 111349. 10.1016/j.celrep.2022.111349.

27. Sardiello, M., Palmieri, M., di Ronza, A., Medina, D.L., Valenza, M., Gennarino, V.A., Di Malta, C., Donaudy, F., Embrione, V., Polishchuk, R.S., et al. (2009). A gene network regulating lysosomal biogenesis and function. Science *325*, 473-477. 10.1126/science.1174447.

28. Puertollano, R., Ferguson, S.M., Brugarolas, J., and Ballabio, A. (2018). The complex relationship between TFEB transcription factor phosphorylation and subcellular localization. EMBO J *37*. 10.15252/embj.201798804.

29. Shariq, M., Khan, M.F., Raj, R., Ahsan, N., and Kumar, P. (2024). PRKAA2, MTOR, and TFEB in the regulation of lysosomal damage response and autophagy. J Mol Med (Berl) *102*, 287-311. 10.1007/s00109-023-02411-7.

30. Settembre, C., Fraldi, A., Medina, D.L., and Ballabio, A. (2013). Signals from the lysosome: a control centre for cellular clearance and energy metabolism. Nat Rev Mol Cell Biol *14*, 283-296. 10.1038/nrm3565.

31. Maejima, I., Takahashi, A., Omori, H., Kimura, T., Takabatake, Y., Saitoh, T., Yamamoto, A., Hamasaki, M., Noda, T., Isaka, Y., and Yoshimori, T. (2013). Autophagy

714 sequesters damaged lysosomes to control lysosomal biogenesis and kidney injury.
715 EMBO J *32*, 2336-2347. 10.1038/emboj.2013.171.
716 32. Endo, A., Fukushima, T., Takahashi, C., Tsuchiya, H., Ohtake, F., Ono, S., Ly, T.,
717 Yoshida, Y., Tanaka, K., Saeki, Y., and Komada, M. (2024). USP8 prevents aberrant NF-
718 kappaB and Nrf2 activation by counteracting ubiquitin signals from endosomes. J Cell
719 Biol *223*. 10.1083/jcb.202306013.
720 33. Endo, A., Komada, M., and Yoshida, Y. (2024). Ubiquitin-mediated endosomal stress: A
721 novel organelle stress of early endosomes that initiates cellular signaling pathways:
722 USP8 serves as a gatekeeper of ubiquitin-mediated endosomal stress to counteract the
723 activation of cellular signaling pathways. Bioessays *46*, e2400127.
724 10.1002/bies.202400127.
725 34. Jia, J., Wang, F., Bhujabal, Z., Peters, R., Mudd, M., Duque, T., Allers, L., Javed, R.,
726 Salemi, M., Behrends, C., et al. (2022). Stress granules and mTOR are regulated by
727 membrane atg8ylation during lysosomal damage. J Cell Biol *221*.
728 10.1083/jcb.202207091.
729 35. Uchimoto, T., Nohara, H., Kamehara, R., Iwamura, M., Watanabe, N., and Kobayashi, Y.
730 (1999). Mechanism of apoptosis induced by a lysosomotropic agent, L-Leucyl-L-Leucine
731 methyl ester. Apoptosis *4*, 357-362. 10.1023/a:1009695221038.
732 36. Liberzon, A., Birger, C., Thorvaldsdottir, H., Ghandi, M., Mesirov, J.P., and Tamayo, P.
733 (2015). The Molecular Signatures Database (MSigDB) hallmark gene set collection.
734 Cell Syst *1*, 417-425. 10.1016/j.cels.2015.12.004.
735 37. Garcia-Alonso, L., Holland, C.H., Ibrahim, M.M., Turei, D., and Saez-Rodriguez, J.
736 (2019). Benchmark and integration of resources for the estimation of human
737 transcription factor activities. Genome Res *29*, 1363-1375. 10.1101/gr.240663.118.
738 38. Badia, I.M.P., Velez Santiago, J., Braunger, J., Geiss, C., Dimitrov, D., Muller-Dott, S.,
739 Taus, P., Dugourd, A., Holland, C.H., Ramirez Flores, R.O., and Saez-Rodriguez, J.
740 (2022). decoupleR: ensemble of computational methods to infer biological activities from
741 omics data. Bioinform Adv *2*, vbac016. 10.1093/bioadv/vbac016.
742 39. Jia, J., Claude-Taupin, A., Gu, Y., Choi, S.W., Peters, R., Bissa, B., Mudd, M.H., Allers,
743 L., Pallikkuth, S., Lidke, K.A., et al. (2020). Galectin-3 Coordinates a Cellular System
744 for Lysosomal Repair and Removal. Dev Cell *52*, 69-87 e68.
745 10.1016/j.devcel.2019.10.025.
746 40. Kulathu, Y., Akutsu, M., Bremm, A., Hofmann, K., and Komander, D. (2009). Two-sided

ubiquitin binding explains specificity of the TAB2 NZF domain. Nat Struct Mol Biol *16*, 1328-1330. 10.1038/nsmb.1731.

41. Kanayama, A., Seth, R.B., Sun, L., Ea, C.K., Hong, M., Shaito, A., Chiu, Y.H., Deng, L., and Chen, Z.J. (2004). TAB2 and TAB3 activate the NF-kappaB pathway through binding to polyubiquitin chains. Mol Cell *15*, 535-548. 10.1016/j.molcel.2004.08.008.

42. Xia, Z.P., Sun, L., Chen, X., Pineda, G., Jiang, X., Adhikari, A., Zeng, W., and Chen, Z.J. (2009). Direct activation of protein kinases by unanchored polyubiquitin chains. Nature *461*, 114-119. 10.1038/nature08247.

43. Hu, M.M., Yang, Q., Zhang, J., Liu, S.M., Zhang, Y., Lin, H., Huang, Z.F., Wang, Y.Y., Zhang, X.D., Zhong, B., and Shu, H.B. (2014). TRIM38 inhibits TNFalpha- and IL-1beta-triggered NF-kappaB activation by mediating lysosome-dependent degradation of TAB2/3. Proc Natl Acad Sci U S A *111*, 1509-1514. 10.1073/pnas.1318227111.

44. Kehl, S.R., Soos, B.A., Saha, B., Choi, S.W., Herren, A.W., Johansen, T., and Mandell, M.A. (2019). TAK1 converts Sequestosome 1/p62 from an autophagy receptor to a signaling platform. EMBO Rep *20*, e46238. 10.15252/embr.201846238.

45. Ogura, M., Shima, T., Yoshimori, T., and Nakamura, S. (2022). Protocols to monitor TFEB activation following lysosomal damage in cultured cells using microscopy and immunoblotting. STAR Protoc *3*, 101018. 10.1016/j.xpro.2021.101018.

46. Scott, O., Saran, E., and Freeman, S.A. (2025). The spectrum of lysosomal stress and damage responses: from mechanosensing to inflammation. EMBO Rep *26*, 1425-1439. 10.1038/s44319-025-00405-9.

47. Bhardwaj, M., Lee, J.J., Versace, A.M., Harper, S.L., Goldman, A.R., Crissey, M.A.S., Jain, V., Singh, M.P., Vernon, M., Aplin, A.E., et al. (2023). Lysosomal lipid peroxidation regulates tumor immunity. J Clin Invest *133*. 10.1172/JCI164596.

48. Raingeaud, J., Whitmarsh, A.J., Barrett, T., Dérijard, B., and Davis, R.J. (1996). MKK3- and MKK6-regulated gene expression is mediated by the p38 mitogen-activated protein kinase signal transduction pathway. Mol Cell Biol *16*, 1247-1255. 10.1128/mcb.16.3.1247.

49. Davis, R.J. (2000). Signal transduction by the JNK group of MAP kinases. Cell *103*, 239-252. 10.1016/s0092-8674(00)00116-1.

50. Okada, M., Matsuzawa, A., Yoshimura, A., and Ichijo, H. (2014). The lysosome rupture-activated TAK1-JNK pathway regulates NLRP3 inflammasome activation. J Biol Chem *289*, 32926-32936. 10.1074/jbc.M114.579961.

51. Ben-Levy, R., Leighton, I.A., Doza, Y.N., Attwood, P., Morrice, N., Marshall, C.J., and Cohen, P. (1995). Identification of novel phosphorylation sites required for activation of MAPKAP kinase-2. Embo j *14*, 5920-5930. 10.1002/j.1460-2075.1995.tb00280.x.

52. Wang, C., Deng, L., Hong, M., Akkaraju, G.R., Inoue, J., and Chen, Z.J. (2001). TAK1 is a ubiquitin-dependent kinase of MKK and IKK. Nature *412*, 346-351. 10.1038/35085597.

53. Tak, P.P., and Firestein, G.S. (2001). NF-kappaB: a key role in inflammatory diseases. J Clin Invest *107*, 7-11. 10.1172/JCI11830.

54. Zein, L., Dietrich, M., Balta, D., Bader, V., Scheuer, C., Zellner, S., Weinelt, N., Vandrey, J., Mari, M.C., Behrends, C., et al. (2025). Linear ubiquitination at damaged lysosomes induces local NFKB activation and controls cell survival. Autophagy, 1-21. 10.1080/15548627.2024.2443945.

55. Zhong, Z., Wen, Z., and Darnell, J.E., Jr. (1994). Stat3: a STAT family member activated by tyrosine phosphorylation in response to epidermal growth factor and interleukin-6. Science *264*, 95-98. 10.1126/science.8140422.

56. Kakuda, K., Ikenaka, K., Kuma, A., Doi, J., Aguirre, C., Wang, N., Ajiki, T., Choong, C.J., Kimura, Y., Badawy, S.M.M., et al. (2024). Lysophagy protects against propagation of alpha-synuclein aggregation through ruptured lysosomal vesicles. Proc Natl Acad Sci U S A *121*, e2312306120. 10.1073/pnas.2312306120.

57. Simonaro, C.M. (2016). Lysosomes, Lysosomal Storage Diseases, and Inflammation. Journal of Inborn Errors of Metabolism and Screening *4*. 10.1177/2326409816650465.

58. Seoane, P.I., Lee, B., Hoyle, C., Yu, S., Lopez-Castejon, G., Lowe, M., and Brough, D. (2020). The NLRP3-inflammasome as a sensor of organelle dysfunction. J Cell Biol *219*. 10.1083/jcb.202006194.

59. Munoz-Planillo, R., Kuffa, P., Martinez-Colon, G., Smith, B.L., Rajendiran, T.M., and Nunez, G. (2013). K(+) efflux is the common trigger of NLRP3 inflammasome activation by bacterial toxins and particulate matter. Immunity *38*, 1142-1153. 10.1016/j.immuni.2013.05.016.

60. Fischer, T.D., Bunker, E.N., Zhu, P.P., Le Guerroue, F., Hadjian, M., Dominguez-Martin, E., Scavone, F., Cohen, R., Yao, T., Wang, Y., et al. (2024). STING induces HOIP-mediated synthesis of M1 ubiquitin chains to stimulate NF-kappaB signaling. EMBO J. 10.1038/s44318-024-00291-2.

61. Harding, O., Holzer, E., Riley, J.F., Martens, S., and Holzbaur, E.L.F. (2023). Damaged

813 mitochondria recruit the effector NEMO to activate NF-kappaB signaling. Mol Cell *83*,
814 3188-3204 e3187. 10.1016/j.molcel.2023.08.005.
815 62. Demichev, V., Messner, C.B., Vernardis, S.I., Lilley, K.S., and Ralser, M. (2020). DIA-
816 NN: neural networks and interference correction enable deep proteome coverage in
817 high throughput. Nat Methods *17*, 41-44. 10.1038/s41592-019-0638-x.
818 63. Tyanova, S., Temu, T., Sinitcyn, P., Carlson, A., Hein, M.Y., Geiger, T., Mann, M., and
819 Cox, J. (2016). The Perseus computational platform for comprehensive analysis of
820 (prote)omics data. Nat Methods *13*, 731-740. 10.1038/nmeth.3901.
821 64. Etoh, K., and Nakao, M. (2023). A web-based integrative transcriptome analysis,
822 RNAseqChef, uncovers the cell/tissue type-dependent action of sulforaphane. J Biol
823 Chem *299*, 104810. 10.1016/j.jbc.2023.104810.
824 65. Perez-Riverol, Y., Bai, J., Bandla, C., Garcia-Seisdedos, D., Hewapathirana, S.,
825 Kamatchinathan, S., Kundu, D.J., Prakash, A., Frericks-Zipper, A., Eisenacher, M., et
826 al. (2022). The PRIDE database resources in 2022: a hub for mass spectrometry-based
827 proteomics evidences. Nucleic Acids Res *50*, D543-D552. 10.1093/nar/gkab1038.
828

Figure legends

Figure 1 | Lysosomal damage has a global impact on the transcriptome and proteome

(A, B) The mean Log_2 fold change (FC, LLOMe 2 h/control) and $-Log_{10}$ *P* value of the transcriptome (A) and proteome (B) in RPE-1 cells are indicated on the x and y axes, respectively. Genes significantly upregulated or downregulated are labeled in red and blue, respectively.

(C) For genes showing significant upregulation in the transcriptome (Log_2 FC >1 and *P* <0.05), the correlation between the mean Log_2 FC of the transcriptome (from A, x axis) and the proteome (from B, y axis) is shown with a coefficient of correlation (R = 0.5899, n = 302).

(D, E) The bubble plots show the outcomes of gene enrichment analyses based on gene ontology molecular function (GOMF) (D) and MSigDB hallmark gene sets (E) for genes upregulated at the protein and RNA levels (top ten and five categories for GOMF and MSigDB hallmark gene sets, respectively). The color and size of the bubbles indicate the *q* value and gene ratio, respectively. The categories related to transcription, cytokine/growth factor, and apoptosis are labeled in red, blue, and green, respectively.

(F) The bubble plot illustrates the DoRothEA regulon-based prediction of transcription factors responsible for the induction of genes upregulated in cells treated with LLOMe (top five transcription factors). The color and size of the bubbles indicate the *q* value and gene ratio, respectively. NF-κB components are labeled in blue.

(G) RPE-1 cells were treated with LLOMe for 2 h and then washed. The total incubation times are indicated. Total cell lysates were subjected to immunoblotting with the indicated antibodies.

(H) Schematic model of the cellular response to lysosomal damage.

Figure 2 | Lysosomal damage activates TAK1 in a ubiquitin- and TAB-dependent manner

(A) RPE-1 cells treated with LLOMe for 5 min were immunostained with the indicated antibodies and DAPI. Scale bar, 20 μm.

(B) Total cell lysates from RPE-1 cells treated with LLOMe for the indicated times were subjected to immunoblotting with the indicated antibodies.

(C) Total cell lysates from RPE-1 cells pre-treated with TAK-243 for 15 min and treated with LLOMe for 15 min were subjected to immunoblotting with the indicated antibodies.

(D) Total cell lysates from RPE-1 cells transfected with the indicated siRNAs and treated with LLOMe for 15 min were subjected to immunoblotting with the indicated antibodies.
(E) HeLa cells stably expressing FLAG-TAB2 WT, dNZF, and E685A were transfected with the indicated siRNAs and treated with LLOMe for 15 min. Total cell lysates were subjected to immunoblotting with the indicated antibodies.

Figure 3 | The TAB–TAK1 pathway activates cytokines and transcription factors in response to lysosomal damage

(A) Heatmap showing the changes in the transcriptome of each sample. Clusters 4 and 5 include the genes upregulated by LLOMe in a TAB- and TAK1-dependent manner.
(B) The bubble plot shows the DoRothEA regulon-based prediction of transcription factors responsible for the induction of genes assigned to clusters 4 and 5 in (A) (top five transcription factors). The color and size of bubbles indicate *q* value and gene ratio, respectively. NF-κB components are labeled in blue.
(C, D) The bubble plots show the outcomes of gene enrichment analyses based on GOMF (C) and MSigDB hallmark gene sets (D) for genes assigned to clusters 4 and 5 in (A) (top five categories). The color and size of the bubbles indicate the *q* value and gene ratio, respectively. The categories related to transcription, cytokine/growth factor, and apoptosis are labeled in red, blue, and green, respectively.
(E) Heatmaps showing the genes upregulated in a TAB- and TAK1-dependent manner within the categories of inflammatory response (left) and transcription-related factors (right). The color intensity indicates the Log_2 FC (LLOMe 2 h/control).
(F) Total cell lysates from RPE-1 cells transfected with the indicated siRNAs, treated with LLOMe for 2 h, and washed for 2 h were subjected to immunoblotting with the indicated antibodies.

Figure 4 | The K63 Ub–TAB–TAK1–IKK–NF-κB pathway induces the expression of cytokines and transcription factors

(A) The mean Log_2 FC (LLOMe 30 min/control) and $-\mathrm{Log}_{10}$ *P* value of the proteome are indicated on the x and y axes, respectively. Proteins significantly upregulated or downregulated are labeled in red and blue, respectively.
(B) IκBα protein abundance determined by mass spectrometry (MS) analysis. The

894 individual values, mean, and standard deviation (SD) of the mean of protein abundance are
895 presented. The mean ± SD values were calculated from two biological replicates. *P <0.05
896 (one-way ANOVA with Dunnett's test).
897 **(C)** Total cell lysates from RPE-1 cells treated with LLOMe for the indicated times were
898 subjected to immunoblotting with the indicated antibodies.
899 **(D)** Total cell lysates from RPE-1 cells pre-treated with TAK-243 for 15 min and treated
900 with LLOMe for 10 min were subjected to immunoblotting with the indicated antibodies.
901 **(E, F)** Total cell lysates from RPE-1 cells transfected with the indicated siRNAs and treated
902 with LLOMe for 10 min were subjected to immunoblotting with the indicated antibodies.
903 **(G)** Schematic model of the cellular signaling pathways activated in response to lysosomal
904 damage.
905

906 **Figure 5 | The K63 Ub–TAB–TAK1–IKK–NF-κB pathway promotes cell survival and**
907 **intercellular signaling**

908 **(A, B)** Total RNA from RPE-1 cells pre-treated with TAK-243 (A) and HS-276 (B) for 15
909 min and treated with LLOMe for 2 h was analyzed by RT-qPCR. Target mRNA levels were
910 normalized to GAPDH mRNA levels; the expression levels in control cells were set to 1.
911 The individual values, mean, and standard error of the mean (SEM) of relative mRNA
912 levels are presented. The mean ± SEM values were calculated from three biological
913 replicates. ****P <0.0001 (one-way ANOVA with Dunnett's test).
914 **(C)** Total RNA from RPE-1 cells transfected with the indicated siRNAs and treated with
915 LLOMe for 2 h was analyzed by RT-qPCR. Target mRNA levels were normalized to
916 GAPDH mRNA levels; the expression levels in cells treated with control siRNA were set to
917 1. The individual values, mean, and SEM of relative mRNA levels are presented. The mean
918 ± SEM values were calculated from three biological replicates. ****P <0.0001 (one-way
919 ANOVA with Dunnett's test).
920 **(D, E)** HeLa cells were pre-treated with TAK-243 or HS-276 for 15 min, treated with
921 LLOMe for 2 h, and washed for 6 h. Total cell lysates were subjected to immunoblotting
922 with the indicated antibodies (D). Cells were stained with propidium iodide (PI), and the
923 fractions of PI-positive cells were assessed using the flow cytometer. Error bars indicate SD
924 (n = 3). ****P < 0.0001 (one-way ANOVA with Dunnett's test) (E).
925 **(F, G)** Total cell lysates from HeLa cells transfected with the indicated siRNAs, treated

with LLOMe for 2 h, and washed for 22 h were subjected to immunoblotting with the indicated antibodies.

(H) RPE-1 cells were stimulated for the indicated times with conditioned media (CM) from RPE-1 cells treated with LLOMe for 30 min and washed for 7.5 h. Total cell lysates were subjected to immunoblotting with the indicated antibodies.

(I, J) RPE-1 cells were stimulated for 15 min with CM from RPE-1 cells transfected with the indicated siRNAs, treated with LLOMe for 30 min, and washed for 7.5 h. Total cell lysates were subjected to immunoblotting with the indicated antibodies.

Figure 6 | Model of the ubiquitin-mediated cellular response to lysosomal damage

Supplementary figure legends

Figure S1

(A) Heatmap showing genes upregulated at both the protein and mRNA levels, as derived from Fig. 1C (top 30 in proteomic upregulation). The color scale represents Log_2 FC (LLOMe 2 h/control).

(B) RNA counts (top) and protein abundance (bottom) of representative genes, as measured by RNA sequencing and MS analysis, respectively. The individual values, mean, and SEM are shown. The mean ± SEM values were calculated from three biological replicates. *P <0.05, ***P <0.001, and ****P <0.0001 (two-tailed Student's t-test).

Figure S2

(A) RPE-1 cells treated with LLOMe for 5 min were immunostained with the indicated antibodies and DAPI. Scale bar, 20 μm.

(B) RPE-1 cells pre-treated with TAK-243 for 15 min and treated with LLOMe for 5 min were immunostained with the indicated antibodies and DAPI. Scale bar, 20 μm.

(C, D) RPE-1 cells treated with GPN (C) and DC661 (D) for 4 h were immunostained with the indicated antibodies and DAPI. Scale bar, 20 μm.

(E) Total cell lysates from RPE-1 cells treated with GPN, DC661, and LLOMe for the indicated times were subjected to immunoblotting with the indicated antibodies.

Figure S3

(A) Scatter plots showing the correlation between the mean Log_2 FC (LLOMe 2 h/control) in cells transfected with siControl (x axis) and siTAB2/3 (y axis) (left), and siControl (x axis) and siTAK1 (y axis) (right).

(B) Venn diagram showing the overlap of genes upregulated by LLOMe treatment in a TAB- and TAK1-dependent manner.

(C, D) The bubble plots show the outcomes of gene enrichment analyses based on GOMF (C) and MSigDB hallmark gene sets (D) for genes upregulated by LLOMe treatment in a TAB- and TAK1-dependent manner (top five categories). The color and size of the bubbles indicate the q value and gene ratio, respectively. The categories related to cytokine/growth factor and apoptosis are labeled in blue and green, respectively.

(E) RNA counts of representative genes, as measured by RNA sequencing. The individual values, mean, and SEM are presented. The mean ± SD values were calculated from three

biological replicates. ****P <0.0001 (one-way ANOVA with Dunnett's test).

Figure S4

(A) The mean Log_2 FC (LLOMe 30 min/control) and $-Log_{10}$ P value of the phosphopeptides are indicated on the x and y axes, respectively. Phosphopeptides significantly upregulated or downregulated are labeled in red and blue, respectively.

(B) Correlation between the mean Log_2 FC (LLOMe 30 min/control) in cells treated with (y axis) or without HS-276 (x axis) is shown for phosphopeptides that were significantly upregulated 30 min after LLOMe treatment (Log_2 FC >1 and P <0.05).

(C) Phosphopeptides abundance measured by MS analysis. The individual values, mean, and SD of the mean of phosphopeptide abundance are shown. The mean ± SD values were calculated from three biological replicates. **P <0.01 and ****P <0.0001 (one-way ANOVA with Dunnett's test).

(D) Total cell lysates from RPE-1 cells treated with LLOMe for the indicated times were subjected to immunoblotting with the indicated antibodies.

(E) Total cell lysates from RPE-1 cells transfected with the indicated siRNAs and treated with LLOMe for 10 min were subjected to immunoblotting with the indicated antibodies.

(F) Total cell lysates from RPE-1 cells pre-treated with BX-795 for 15 min and treated with LLOMe for 10 min were subjected to immunoblotting with the indicated antibodies.

(G) Total cell lysates from RPE-1 cells transfected with the indicated siRNAs and treated with LLOMe for 10 min were subjected to immunoblotting with the indicated antibodies.

Figure S5

(A) Total cell lysates from RPE-1 cells pre-treated with TAK-243 or HS-276 for 15 min, treated with LLOMe for 2 h, and washed for 6 h were subjected to immunoblotting with the indicated antibodies.

(B) Total cell lysates from HeLa cells pre-treated with JNK-IN-8 for 15 min, treated with LLOMe for 2 h, and washed for 10 h were subjected to immunoblotting with the indicated antibodies.

Supplementary table titles

Table S1 | Transcriptome analysis LLOMe 2 h

Table S2 | Proteome analysis LLOMe 2 h

1003 **Table S3 | Correlation of Transcriptome and Proteome LLOMe 2 h**

1004 **Table S4 | Transcriptome analysis RNAi LLOMe 2 h**

1005 **Table S5 | Proteome analysis LLOMe 30 min**

1006 **Table S6 | Phosphoproteome analysis with HS-276**

1007

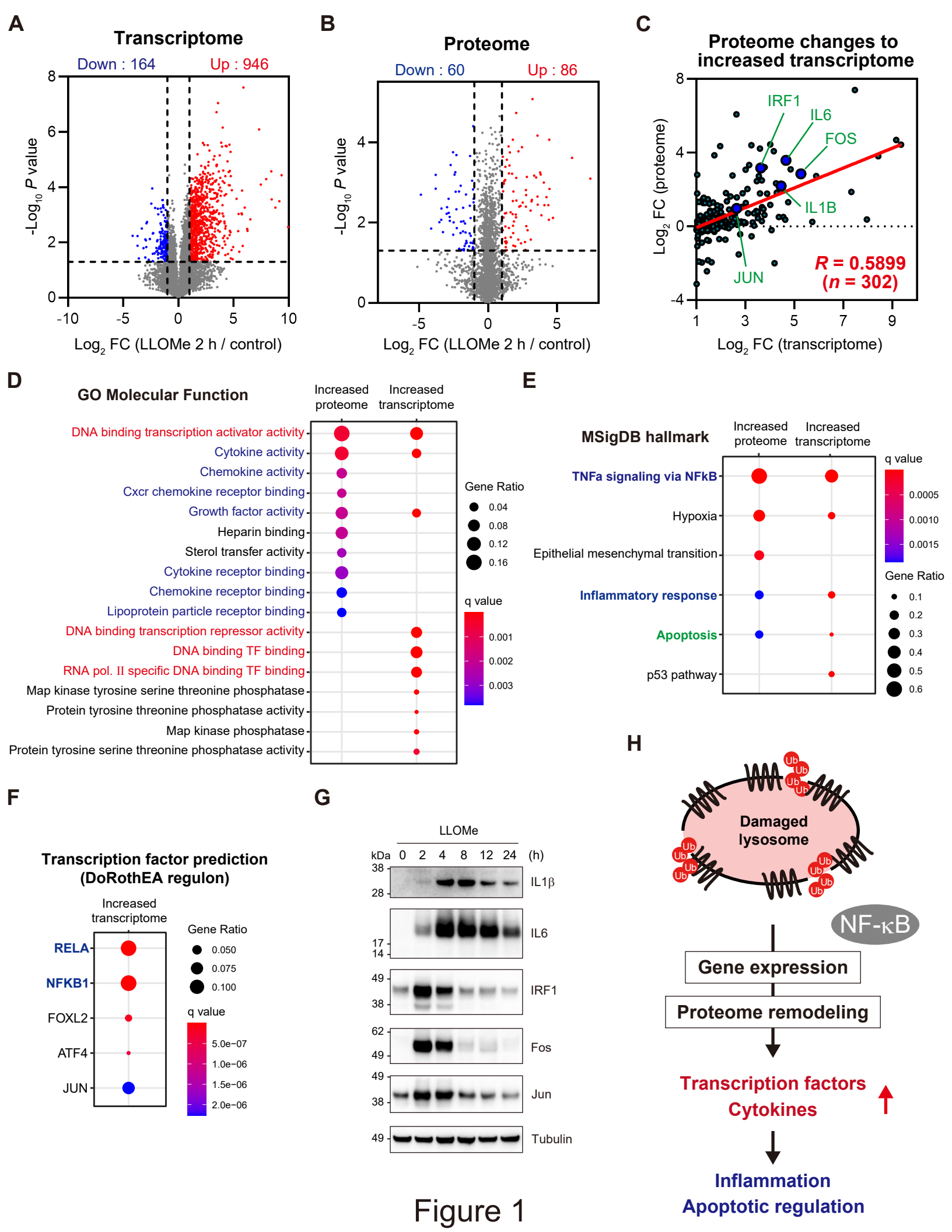
A
Transcriptome
Down : 164
Up : 946
-Log10 P value
Log2 FC (LLOMe 2 h / control)
B
Proteome
Down : 60
Up : 86
-Log10 P value
Log2 FC (LLOMe 2 h / control)
C
Proteome changes to increased transcriptome
IRF1
IL6
FOS
IL1B
JUN
R = 0.5899
(n = 302)
Log2 FC (proteome)
Log2 FC (transcriptome)
D
GO Molecular Function
Increased proteome
Increased transcriptome
DNA binding transcription activator activity
Cytokine activity
Chemokine activity
Cxcr chemokine receptor binding
Growth factor activity
Heparin binding
Sterol transfer activity
Cytokine receptor binding
Chemokine receptor binding
Lipoprotein particle receptor binding
DNA binding transcription repressor activity
DNA binding TF binding
RNA pol. II specific DNA binding TF binding
Map kinase tyrosine serine threonine phosphatase
Protein tyrosine threonine phosphatase activity
Map kinase phosphatase
Protein tyrosine serine threonine phosphatase activity
Gene Ratio
q value
E
MSigDB hallmark
Increased proteome
Increased transcriptome
TNFa signaling via NFkB
Hypoxia
Epithelial mesenchymal transition
Inflammatory response
Apoptosis
p53 pathway
q value
Gene Ratio
F
Transcription factor prediction
(DoRothEA regulon)
Increased transcriptome
RELA
NFKB1
FOXL2
ATF4
JUN
Gene Ratio
q value
G
LLOMe
kDa
(h)
IL1β
IL6
IRF1
Fos
Jun
Tubulin
H
Damaged lysosome
Ub
NF-κB
Gene expression
Proteome remodeling
Transcription factors
Cytokines
Inflammation
Apoptotic regulation

Figure 1

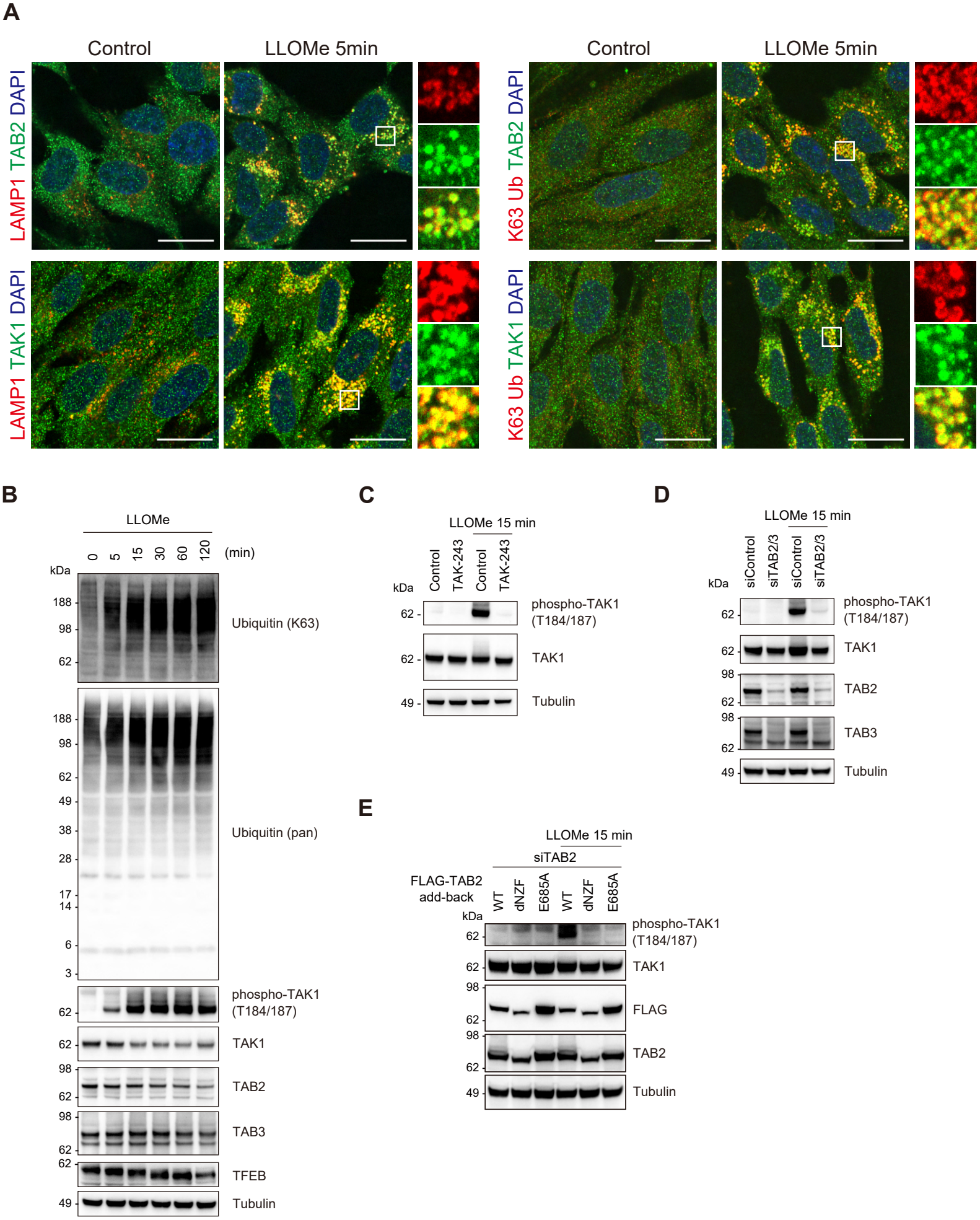
A
Control
LLOMe 5min
Control
LLOMe 5min
LAMP1 TAB2 DAPI
K63 Ub TAB2 DAPI
LAMP1 TAK1 DAPI
K63 Ub TAK1 DAPI
B
LLOMe
0
5
15
30
60
120
(min)
kDa
188
98
62
Ubiquitin (K63)
188
98
62
49
38
28
17
14
6
3
Ubiquitin (pan)
62
phospho-TAK1
(T184/187)
62
TAK1
98
62
TAB2
98
62
TAB3
62
TFEB
49
Tubulin
C
LLOMe 15 min
Control
TAK-243
Control
TAK-243
kDa
62
phospho-TAK1
(T184/187)
62
TAK1
49
Tubulin
D
LLOMe 15 min
siControl
siTAB2/3
siControl
siTAB2/3
kDa
62
phospho-TAK1
(T184/187)
62
TAK1
98
62
TAB2
98
62
TAB3
49
Tubulin
E
LLOMe 15 min
siTAB2
FLAG-TAB2
add-back
WT
dNZF
E685A
WT
dNZF
E685A
kDa
62
phospho-TAK1
(T184/187)
62
TAK1
98
62
FLAG
98
62
TAB2
49
Tubulin

Figure 2

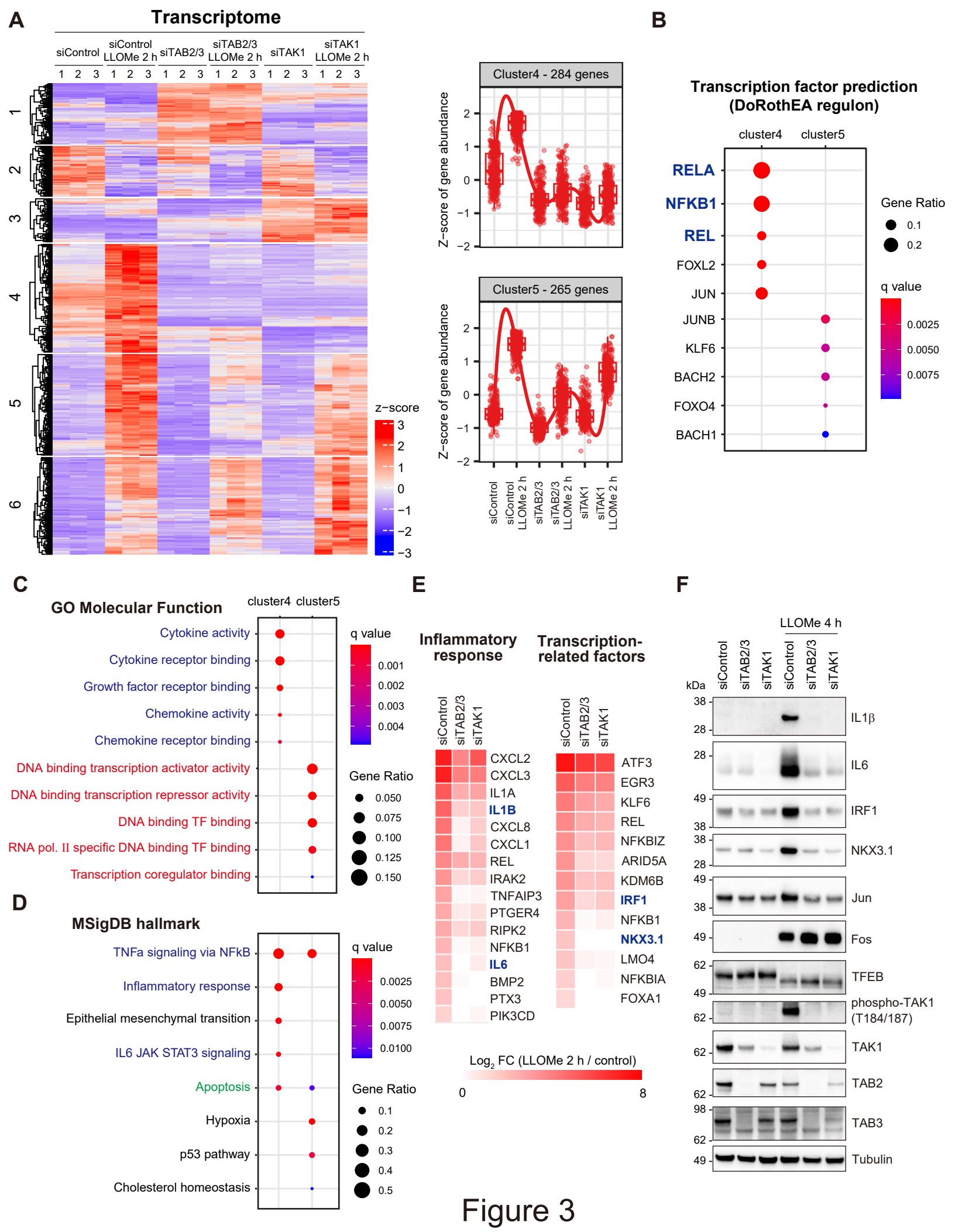
A
Transcriptome
siControl
siControl LLOMe 2 h
siTAB2/3
siTAB2/3 LLOMe 2 h
siTAK1
siTAK1 LLOMe 2 h
z−score
Cluster4 - 284 genes
Cluster5 - 265 genes
Z−score of gene abundance
B
Transcription factor prediction (DoRothEA regulon)
cluster4
cluster5
RELA
NFKB1
REL
FOXL2
JUN
JUNB
KLF6
BACH2
FOXO4
BACH1
Gene Ratio
q value
C
GO Molecular Function
Cytokine activity
Cytokine receptor binding
Growth factor receptor binding
Chemokine activity
Chemokine receptor binding
DNA binding transcription activator activity
DNA binding transcription repressor activity
DNA binding TF binding
RNA pol. II specific DNA binding TF binding
Transcription coregulator binding
D
MSigDB hallmark
TNFa signaling via NFkB
Inflammatory response
Epithelial mesenchymal transition
IL6 JAK STAT3 signaling
Apoptosis
Hypoxia
p53 pathway
Cholesterol homeostasis
E
Inflammatory response
Transcription-related factors
siControl
siTAB2/3
siTAK1
CXCL2
CXCL3
IL1A
IL1B
CXCL8
CXCL1
REL
IRAK2
TNFAIP3
PTGER4
RIPK2
NFKB1
IL6
BMP2
PTX3
PIK3CD
ATF3
EGR3
KLF6
REL
NFKBIZ
ARID5A
KDM6B
IRF1
NFKB1
NKX3.1
LMO4
NFKBIA
FOXA1
Log2 FC (LLOMe 2 h / control)
F
LLOMe 4 h
kDa
IL1β
IL6
IRF1
NKX3.1
Jun
Fos
TFEB
phospho-TAK1 (T184/187)
TAK1
TAB2
TAB3
Tubulin

Figure 3

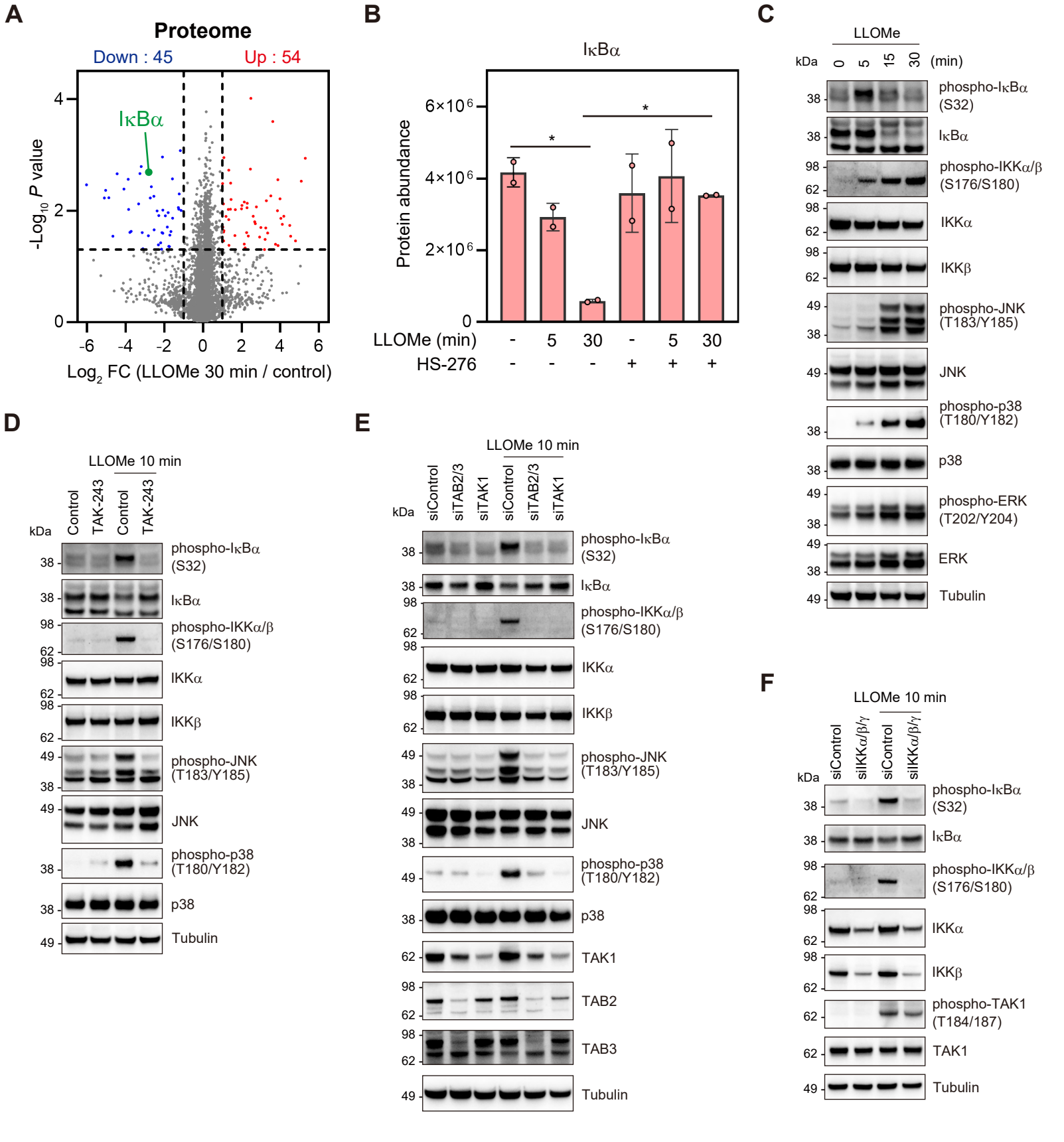
A
Proteome
Down : 45
Up : 54
IκBα
-Log10 P value
Log2 FC (LLOMe 30 min / control)
B
IκBα
Protein abundance
6×10^6
4×10^6
2×10^6
0
LLOMe (min) - 5 30 - 5 30
HS-276 - - - + + +
C
LLOMe
kDa 0 5 15 30 (min)
phospho-IκBα (S32)
IκBα
phospho-IKKα/β (S176/S180)
IKKα
IKKβ
phospho-JNK (T183/Y185)
JNK
phospho-p38 (T180/Y182)
p38
phospho-ERK (T202/Y204)
ERK
Tubulin
D
LLOMe 10 min
Control
TAK-243
Control
TAK-243
kDa
phospho-IκBα (S32)
IκBα
phospho-IKKα/β (S176/S180)
IKKα
IKKβ
phospho-JNK (T183/Y185)
JNK
phospho-p38 (T180/Y182)
p38
Tubulin
E
LLOMe 10 min
siControl
siTAB2/3
siTAK1
siControl
siTAB2/3
siTAK1
kDa
phospho-IκBα (S32)
IκBα
phospho-IKKα/β (S176/S180)
IKKα
IKKβ
phospho-JNK (T183/Y185)
JNK
phospho-p38 (T180/Y182)
p38
TAK1
TAB2
TAB3
Tubulin
F
LLOMe 10 min
siControl
siIKKα/β/γ
siControl
siIKKα/β/γ
kDa
phospho-IκBα (S32)
IκBα
phospho-IKKα/β (S176/S180)
IKKα
IKKβ
phospho-TAK1 (T184/187)
TAK1
Tubulin
G
Damaged lysosome
Ub
TAB2/3
TAK1
P
IKK
P
Degradation
IκBα
P
Activation
NF-κB

Figure 4

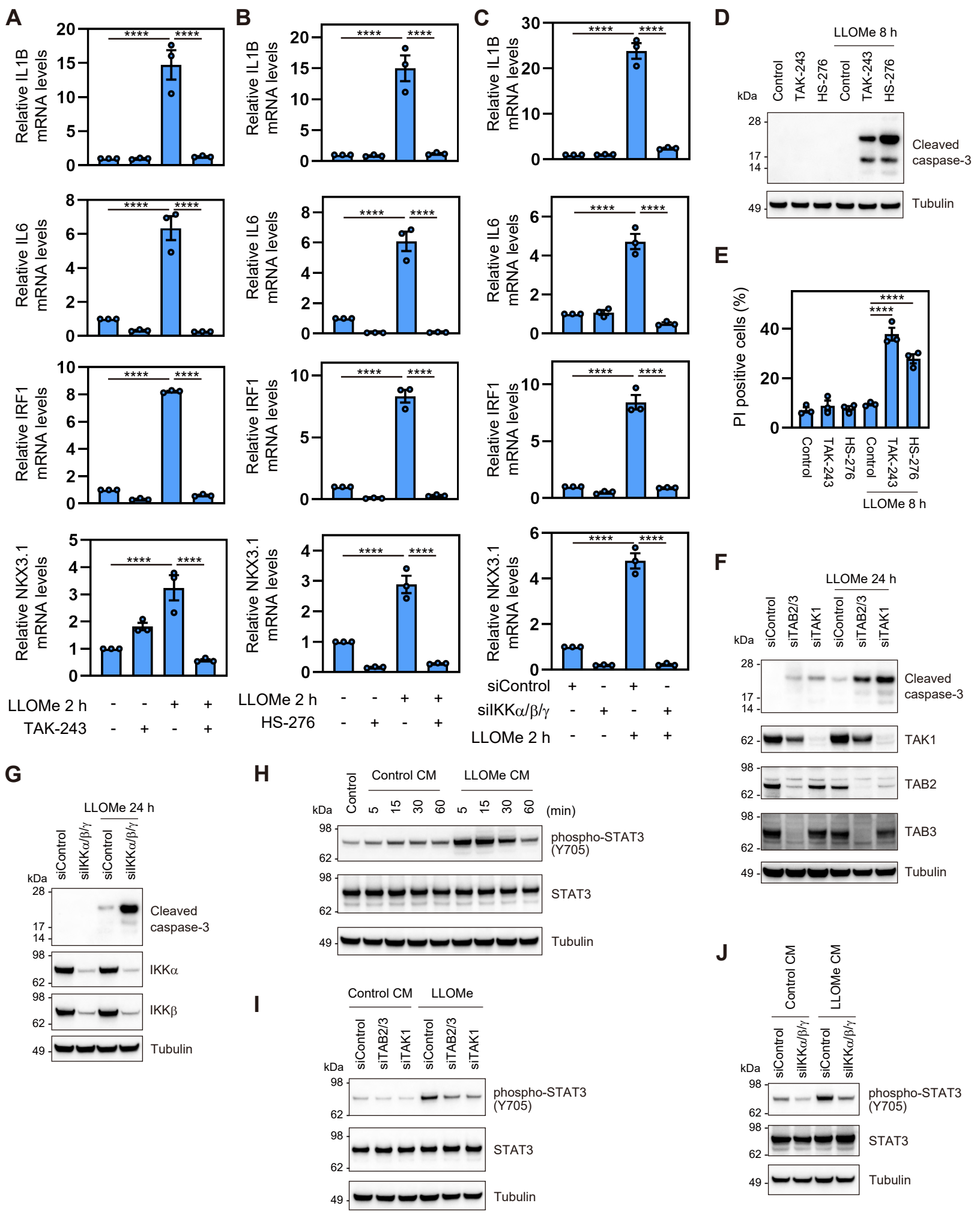
A
B
C
D
E
F
G
H
I
J
Relative IL1B mRNA levels
Relative IL6 mRNA levels
Relative IRF1 mRNA levels
Relative NKX3.1 mRNA levels
****
LLOMe 2 h
TAK-243
HS-276
siControl
siIKKα/β/γ
LLOMe 8 h
Control
TAK-243
HS-276
kDa
Cleaved caspase-3
Tubulin
PI positive cells (%)
LLOMe 24 h
siTAB2/3
siTAK1
TAK1
TAB2
TAB3
IKKα
IKKβ
Control CM
LLOMe CM
LLOMe
(min)
phospho-STAT3 (Y705)
STAT3

Figure 5

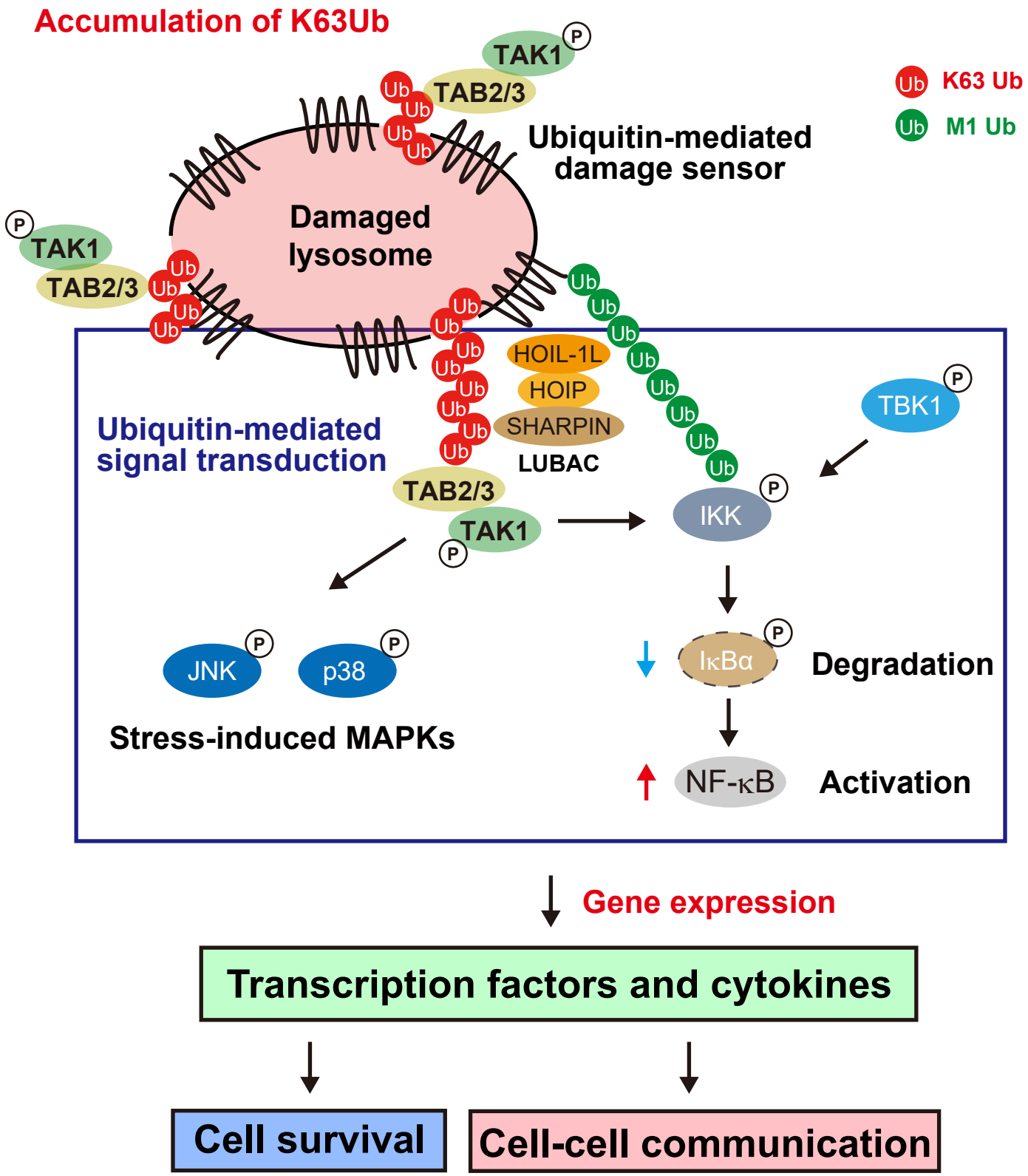
Accumulation of K63Ub
TAK1
P
TAB2/3
Ub
K63 Ub
M1 Ub
Ubiquitin-mediated
damage sensor
Damaged
lysosome
TAK1
TAB2/3
HOIL-1L
HOIP
SHARPIN
LUBAC
TBK1
Ubiquitin-mediated
signal transduction
TAB2/3
TAK1
IKK
JNK
p38
Stress-induced MAPKs
IκBα
Degradation
NF-κB
Activation
Gene expression
Transcription factors and cytokines
Cell survival
Cell-cell communication

Figure 6

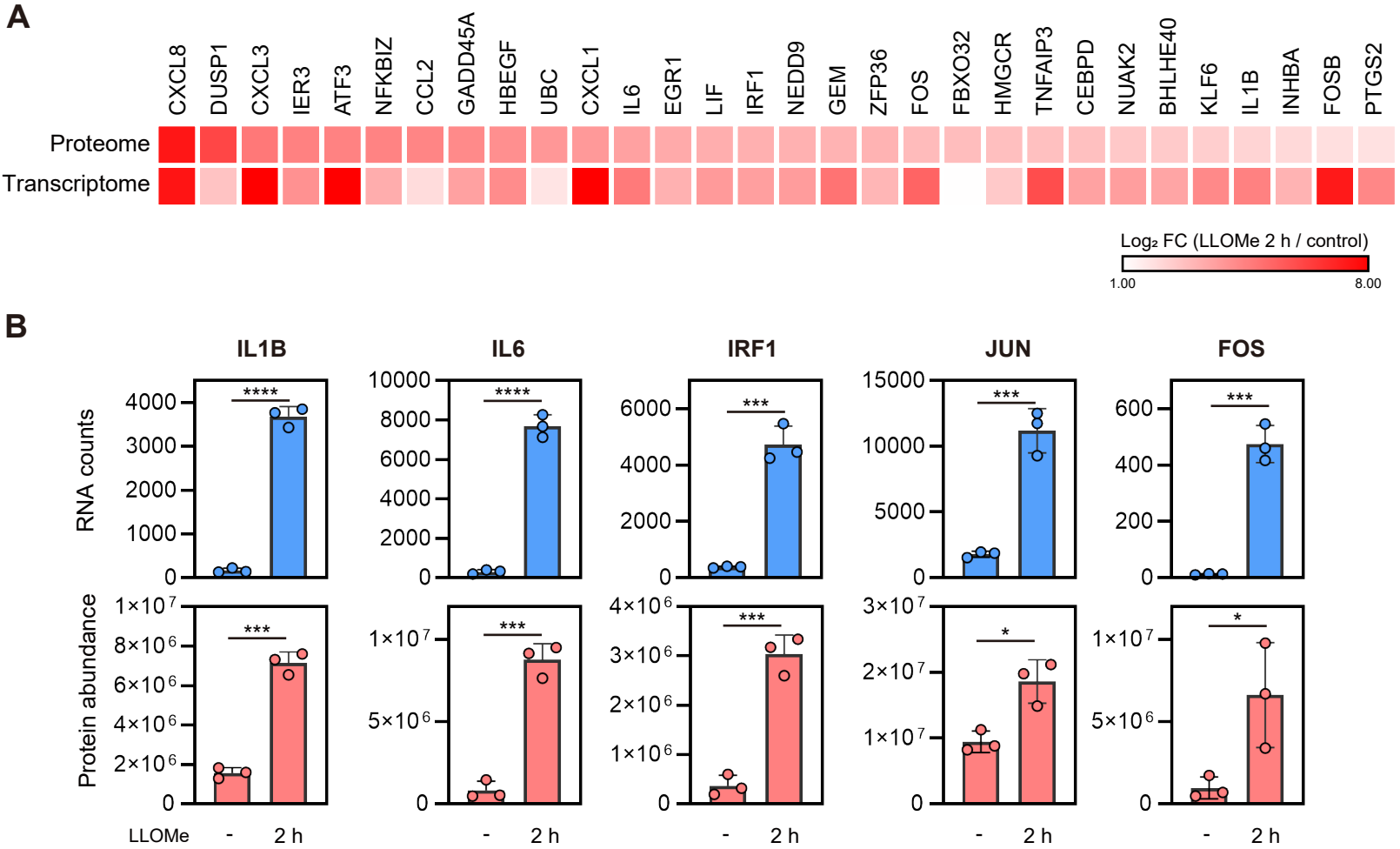

Supplement figure 1

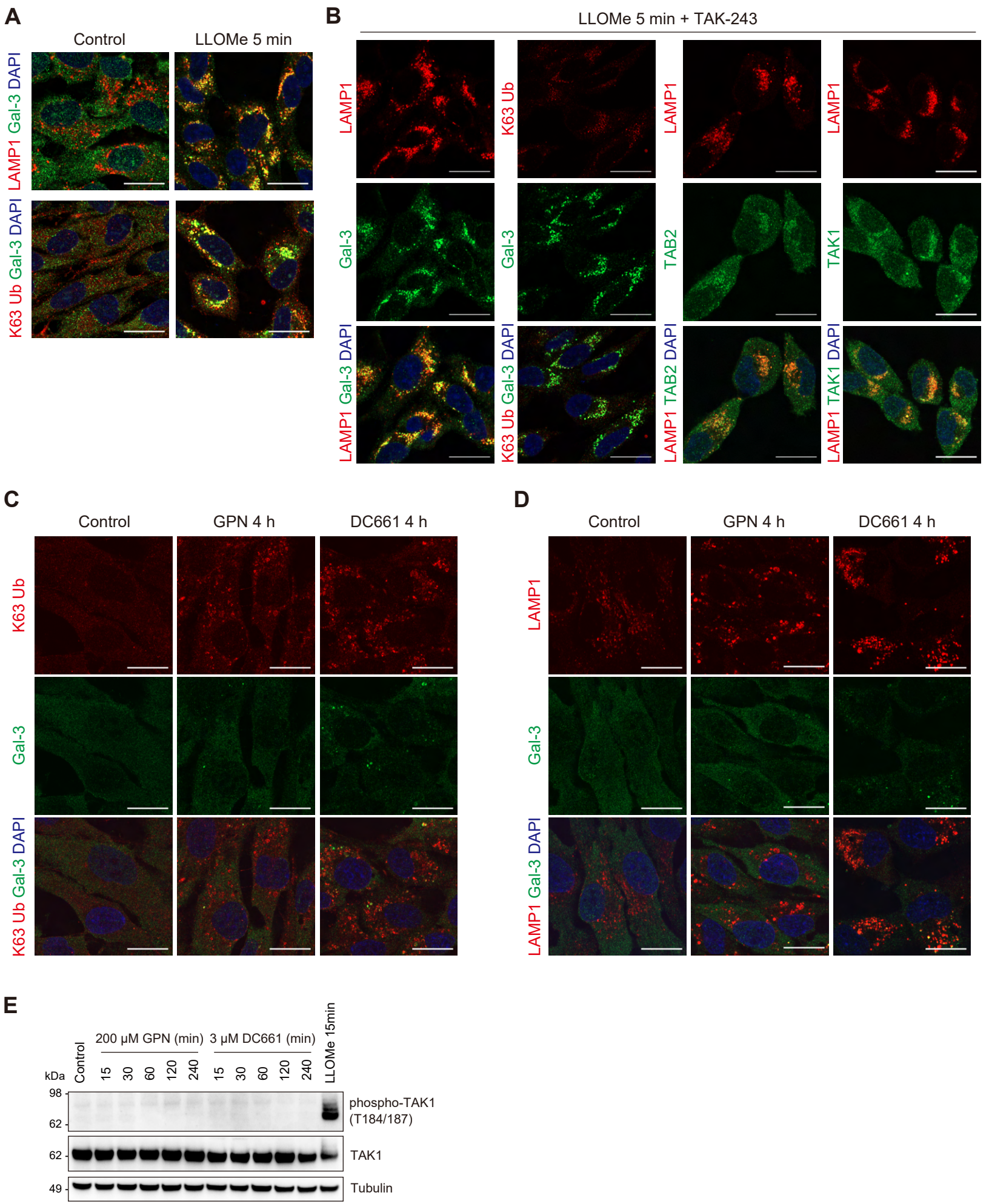

Supplement figure 2

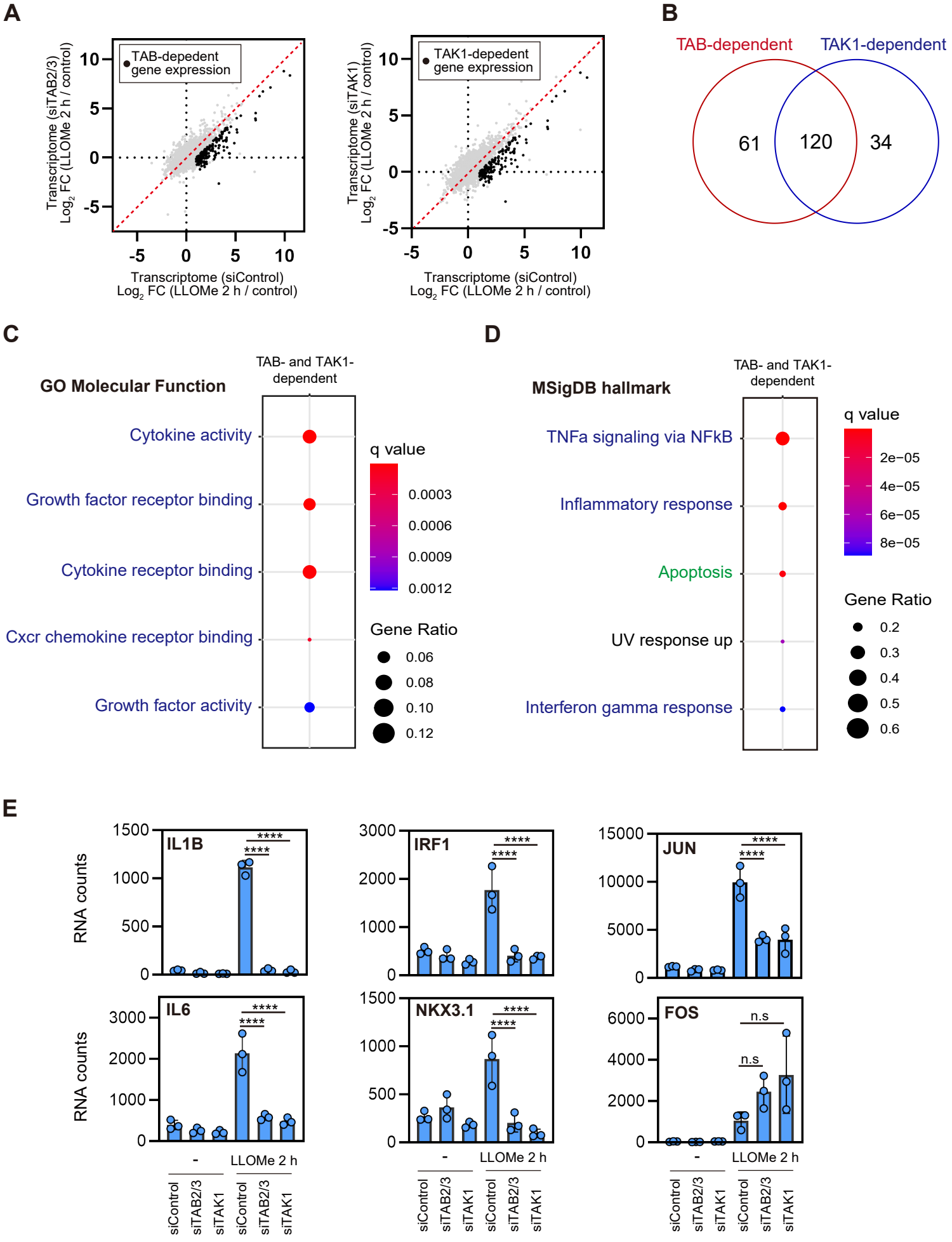

Supplement figure 3

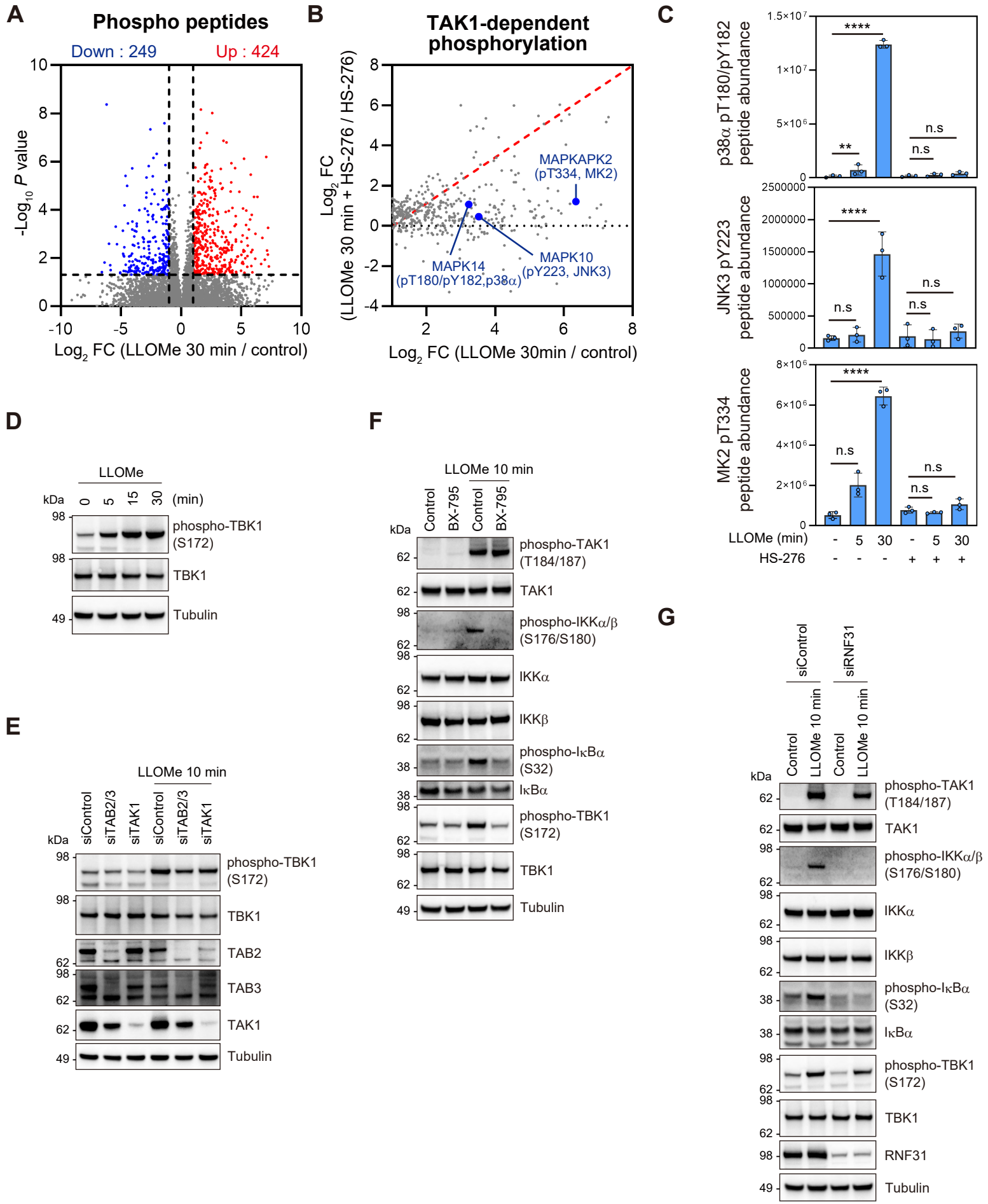

Supplement figure 4

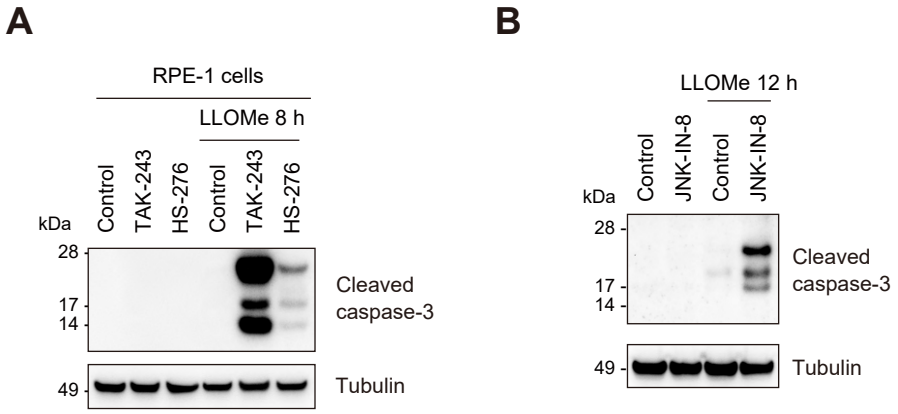

Supplement figure 5